A MULTILEVEL METHOD FOR MESHLESS SOLUTION OF THE POISSON EQUATION IN HEAT TRANSFER AND FLUID FLOW

BY

ANAND RADHAKRISHNAN

THESIS

Submitted in partial fulfillment of the requirements
for the degree of Master of Science in Mechanical Engineering
with a concentration in Computational Science and Engineering
in the Graduate College of the
University of Illinois Urbana-Champaign, 2021

Urbana, Illinois

Advisor:

Professor Surya Pratap Vanka

ABSTRACT

Meshless methods using radial basis functions (RBF) are an attractive alternative to grid based methods for solving partial differential equations in complex geometries. Gaussian, Multiquadratics and inverse Multiquadratics are some of the more popular RBF's, but the require a shape paramter for a stable and accurate solution and also face stagnation issues. Recently, Polyharmonic splines (PHS) with appended polynomials have overcome the aforementioned issues and offer spectral convergence of the discretization errors with the degree of appended polynomials. In this thesis, we present a non-nested multilevel algorithm using the PHS-RBF meshless method for the soluution of the Poisson equation, which commonly arises in numerous heat transfer and fluid flow applications. The PHS-RBF discretization of the Poisson equation leads to a sparse set of equations with unknown variables at each of the scattered point. The non-nested multilevel algorithm solves this set of equations by restricting and prolongating the values and corrections between multiple independently generated coarse set of points by making use of RBF interpolation. The performance of this algorithm is tested for the Poisson equation in three model geometries, using manufactured solutions. Rapid convergence of the residual is observed with Dirichlet boundary conditions using Successive Over-Relaxation(SOR) as the relaxation scheme . However, convergence is seen to be quite modest for the all-Neumann boundary condition, but this poor convergence is ameliorated by using the multilevel algorithm as a preconditioner to the GMRES, which is a Krylov Subspace Projection (KSP) method. This rapid convergence of the all-Neumann equation is then applied to the pressure Poisson equation arising in the fractional step method, with explicit convection and explicit diffusion. We demonstrate fast convergence, both with refinement of number of points and degree of appended polynomials, for various fluid flow problems in complex domains with high accuracy using the meshless fractional step algorithm.

ACKNOWLEDGEMENTS

I would like to extend my gratitude to everyone who helped and supported me during the course of this research project. Firstly, I would like to thank my advisor Prof. Surya Pratap Vanka for his helpful guidance and patience. I would also like to thank Dr. Shantanu Shahane for his meaningful inputs throughout the research project. Lastly, I would also thank Michael Xu for his contributions in developing the code for this project.

Table of Contents

Chapter 1

Introduction

Various methodologies, such as finite volume and finite element methods on unstructured grids and spectral element methods exist for the solution of Navier-Stokes equations in complex domains. While Unstructured FVM's are popular in commercial software, these methods are often limited by second-order accuracy unless complex reconstruction schemes are devised. Thus, to obtain high-order accurate solutions, the grid size has to be extremely small, which leads to long computational times. Alternatives such as spectral domain and spectral element methods require placement of grid points at pre-determined Gauss-Lobatto points, thus restricting local resolution and limiting the time step based on the CFL number. Spectral methods are also often times global, which leads to a full matrix as opposed to sparse, thus requiring tensor product formulation to reduce computational intensity, which makes them less favourable for complex geometries.

Smoothed particle hydrodynamics (Monaghan, 2012; Ye et al., 2019; Zhang et al., 2017), generalized finite difference method (Perrone and Kao, 1975; Liszka and Orkisz, 1980; Gavete et al., 2017), reproducing kernel particle method (Liu et al., 1995; Huang, 2020), element-free Galerkin method (Belytschko et al., 1994; Abbaszadeh et al., 2020; Zhang et al., 2009), hp-clouds (Liszka et al., 1996; Duarte, 1996; Duarte and Oden, 1996), partition of unity (Chen et al., 2006; Melenk and Babuška, 1996; Babuška and Melenk, 1997), finite point method (Boroomand et al., 2009; Oñate et al., 1996, 2000) and radial basis function based finite difference (RBF-FD) method are some of the popular meshless methods. Meshless methods only require scattered points for discretization over any domain, thus eliminating the need for faces and control volumes as in the case of FVM. Hardy (1971) proposed the RBF methodology for a cartography application which required a scattered node interpolation.

Later, Kansa (1990c,d) showed that RBF interpolants can be used to numerically solve PDE's with a globally connected multiquadratic(MQ) function, which leads to an ill-conditioned full matrix as the number of points increased. Kansa and Hon (2000) addresed this problem by block partitioning strategy with preconditioners which help reduce the condition number of the global matrix. Shu et al. (2003) used a local MQ method in which derivatives are approximated using a local cloud of points, much like the finite difference method, which leads to a global sparse matrix with an improved condition number.

Some of the common RBFs previously considered for solution of partial differential equations are as follows:

$$\begin{aligned}
\text{Multiquadrics (MQ): } \phi(\boldsymbol{r}) &= (\boldsymbol{r}^2 + c^2)^{1/2} \\
\text{Inverse Multiquadrics (IMQ): } \phi(\boldsymbol{r}) &= (\boldsymbol{r}^2 + c^2)^{-1/2} \\
\text{Gaussian: } \phi(\boldsymbol{r}) &= \exp\left(\frac{-\boldsymbol{r}^2}{\sigma^2}\right) \\
\text{Polyharmonic Splines (PHS): } \phi(\boldsymbol{r}) &= \boldsymbol{r}^{2a+1},\ a \in N \\
\text{Thin Plate Splines (TPS): } \phi(\boldsymbol{r}) &= \boldsymbol{r}^{2a} log(\boldsymbol{r}),\ a \in N
\end{aligned} \tag{1.1}$$

where r is the magnitude of the distance between two points. The first three radial basis functions need specification of a shape factor c or σ which controls the shape of the RBF.

A variable $f(\boldsymbol{x})$ is interpolated as:

$$f(\boldsymbol{x}) = \sum_{i=1}^{N} \alpha_i \phi(||\boldsymbol{x} - \boldsymbol{x_i}||_2) \tag{1.2}$$

where the symbol N denotes the number of points used in the interpolation 'cloud' for point $\boldsymbol{x}$ and α_i denote the weighting coefficients.

This makes them less ideal, as this shape parameter influences both the degree of accuracy as well as the condition number of the matrix. Large values of the shape parameter lead to highly accurate but ill-conditioned matrices whereas smaller values limit the degree of accuracy at the cost of a well-conditioned system. Thus, prescription of an optimum value of the shape parameter is one of the cardinal issues in the robust use of RBFs for interpolation (Buhmann, 2003; Franke and Nielson, 1980). Furthermore, the shape parameter can lead to

saturation issues, wherein the discretization errors tend to flatline beyond a certain degree of refinement.

Subsequently, Polyharmonic Splines (PHS) in recent years have emerged as a popular solution to the previous issues posed by the shape parameters, which have no such dependency. The saturation phenomenon mentioned above can be overcome by appending polynomials to the PHS (Shahane et al., 2020; Flyer et al., 2016) thus leading to high-order accuracy as well as a well-conditioned sparse matrix at the cost of a slightly higher cloud size and computational work. The degree of accuracy of the PHS-RBF method can be improved by increasing the degree of the appended polynomial as well as decreasing the spacing between points which is akin to (h-p) refinement used in finite element methods. Bayona (2019) compared a local weighted least squares approach with polynomial basis and the PHS–RBF method for interpolation and derivative approximation. The choice of weighting function is a difficulty in the least squares approach and was found to fail at high polynomial degrees. Hence they inferred that the PHS–RBF method is superior. Jančič et al. (2019) used the PHS–RBF method for solution of the Poisson equation in two and three dimensions and demonstrated the increasing order of accuracy with polynomial degree. Gunderman et al. (2020) solved the advection equation on spherical geometries using the PHS–RBF method. They added a small artificial diffusion term to the hyperbolic equation to stabilize the method.

The aforementioned literature survey indicates the effectiveness and advantages of using the PHS-RBF method to solve fluid flow and heat transfer problems. The sparse linear system arising from the PHS-RBF discretization usually results in fairly high condition numbers, particularly for higher appended polynomial degrees. This results in slow convergence of conventional point solvers such as Damped Jacobi and SOR, especially for the low frequency components of the errors. This motivates the study of multilevel methods to overcome this issue of poor convergence.

Multilevel methods(Brandt, 1977; Trottenberg et al., 2000; Briggs et al., 2000; Yavneh, 2006; Stüben and Trottenberg, 1982) have been extensively demonstrated to provide optimal iterative convergence of discretized elliptic partial differential equations such as the Poisson equation encountered in numerous engineering problems (Bairstow and Berry, 1919; Bateman, 1938; Shimada et al., 1991; Harlow and Welch, 1965; Pöplau and Van Rienen, 2001).

By restricting residuals from fine to coarse levels, solving them on coarser levels, and prolongating corrections to the finer levels, multilevel methods provide optimal smoothing of the high frequency errors on the finer levels and the low frequency errors on the coarser levels. The traditional multilevel method (Brandt, 1977) uses nested refinement in which a finer grid is generated by subdividing a coarser grid. In such grids, restriction and prolongation can be performed easily by using linear interpolation. However, when the fine level is arbitrary, this approach does not work. In such a case, several fine grid cells (finite volumes) can be combined to make a coarser cell. Such 'agglomeration' multilevel procedures have been developed for Poisson equation (Koobus et al., 1994; Chan et al., 1998), for Euler (Venkatakrishnan and Mavriplis, 1995; Lallemand et al., 1992; Bassi et al., 2012), and Navier-Stokes (Langer, 2014; Mavriplis and Venkatakrishnan, 1996; Carré, 1997) equations governing fluid flows. A similar technique is also implemented under the name Additive Correction Multigrid (ACM) (Settari and Aziz, 1973; Hutchinson et al., 1988) in which uniform corrections to the fine grid variables are obtained by solving correction equations on coarser grids generated by combining cells. A more general technique for arbitrary sets of linear equations is the Algebraic Multigrid (AMG) method pioneered by Brandt (1986); Ruge and Stüben (1987) and implemented as black-box multigrid software (Yang et al., 2002; Dendy, 1982). The algebraic multigrid technique coarsens the equation system by examining the strengths of the coefficients, and hence results in efficient coarsening strategies consistent with point iterative solvers. Lastly, non-nested multigrid techniques (Bittencourt et al., 2001, 2002; Antonietti and Pennesi, 2019) have also been developed as alternatives to agglomeration and additive correction multigrid methods. The advantage of non-nested multigrid methods is that the discretization operator on coarser levels can be constructed directly by the governing equation (as in nested grids), and therefore the multigrid convergence can be optimal. However, because the grids are not nested, several independent grids need to be generated with restriction/prolongation operators constructed from multi-dimensional interpolation formulae. Recently, Katz and Jameson (2009) used multiquadrics to discretize the compressible flow equations and accelerated the convergence to steady state by a multilevel meshless method. The coarse sets in their method were generated by a special coarsening algorithm.

The desired result for a multigrid method is to obtain convergence which is independent

of grid size for a discrete problem. The iteration count in a multigrid method is limited only by the convergence of the low frequency errors for a relaxation scheme on the coarsest level. Multigrid methods can also be considered as preconditioners to iterative solvers (Wienands et al., 2000; Evstigneev, 2019; Elman et al., 2001; Erlangga et al., 2006; Xu, 1996), lowering the condition number of the iteration matrix to achieve fast convergence. Multigrid methods have been used for solving sets of coupled equations such as those of fluid flow employing either decoupled or coupled solution of the Navier-Stokes equations (Vanka, 1986; John and Tobiska, 2000; Thompson and Ferziger, 1989; Paisley, 1999; Sivaloganathan and Shaw, 1988). For external flows on unstructured grids, agglomeration multigrid with Runge-Kutta time marching schemes have been developed (Mavriplis and Jameson, 1990).

The contributions of this thesis are as follows. We develop a non-nested multilevel meshless method for the Poisson equation discretized by the PHS-RBF method on a complex domain. For a given set of fine points, we independently generate coarse level of points and construct PHS-RBF based Restriction/Prolongation operators to interpolate variables, residuals and corrections between these levels. We use Successive Over-Relaxation (SOR) as the relaxation scheme and examine the convergence of the Poisson equation for Dirichlet and all-Neumann boundary conditions for both 2D and 3D problems. The accuracy of the solution is examined by using a manufactured solution with varying wavenumber. Also, to get rid of the null space in the all-Neumann case, we regularise the equations by adding a constraint, thus making the system well-conditioned.

Once we observe satisfactory convergence of the Poisson equation for all-Neumann boundary conditions, we use it to solve the time-dependent Navier-Stokes equations for incompressible flows on complex domains. We apply the non-nested multilevel solver to the pressure Poisson equation (PPE) which arises as part of the meshless fractional step method. We first demonstrate accuracy by applying the algorithm to two problems with analytical solutions and then use it to investigate two other complex flows. The discretization accuracy in the latter case is examined by treating the numerical solution on a very fine level as the true solution for coarser levels.

Chapter 2

Theory

2.1 The PHS-RBF meshless method

The PHS-RBF interpolates a function $f(\boldsymbol{x})$ whose values are known at scattered points using weighted kernels as:

$$f(\boldsymbol{x}) = \sum_{i=1}^{N} \alpha_i \phi(||\boldsymbol{x} - \boldsymbol{x_i}||_2) \tag{2.1}$$

where ϕ is the polyharmonic spline function given as:

$$\phi(||\boldsymbol{x} - \boldsymbol{x_i}||_2) = ||\boldsymbol{x} - \boldsymbol{x_i}||_2^{2p+1} \tag{2.2}$$

and p = 1,2,3, etc. Further, as mentioned earlier, PHS are appended with number of monomials, the number given by $\binom{l+d}{d}$, where l is the desired highest degree of the monomial and d is the dimension of the problem. Thus, eq. (2.1) is extended as:

$$f(\boldsymbol{x}) = \sum_{i=1}^{N} \alpha_i \phi(||\boldsymbol{x} - \boldsymbol{x_i}||_2) + \sum_{j=1}^{M} \gamma_j P_j(\boldsymbol{x}) \tag{2.3}$$

The RBF $\phi(||\boldsymbol{x} - \boldsymbol{x_i}||_2)$ is a scalar function of the Euclidian distance between the points irrespective of the problem dimension. $P_j(\boldsymbol{x})$ denotes the j^{th} degree monomial which is weighted by the coefficient γ_j. The (N+M) variables in $\boldsymbol{\alpha}$ and $\boldsymbol{\gamma}$ are determined by collocating the variables at the cloud points and satisfying a constraint equation for each appended monomial.

$$\sum_{i=1}^{N} \alpha_i P_j(\boldsymbol{x_i}) = 0; \quad j = 1, 2, ..., M \tag{2.4}$$

Usually, the total number of cloud points N is selected to be a multiple (around twice) of the number of monomials. The collocation equations and constraints for $\boldsymbol{\alpha}$ and $\boldsymbol{\gamma}$ can be written as:

$$\begin{bmatrix} \boldsymbol{\Phi} & \boldsymbol{P} \\ \boldsymbol{P}^T & \boldsymbol{0} \end{bmatrix} \begin{bmatrix} \boldsymbol{\alpha} \\ \boldsymbol{\gamma} \end{bmatrix} = \begin{bmatrix} \boldsymbol{f} \\ \boldsymbol{0} \end{bmatrix} \tag{2.5}$$

or,

$$\begin{bmatrix} \boldsymbol{D} \end{bmatrix} \begin{bmatrix} \boldsymbol{\alpha} \\ \boldsymbol{\gamma} \end{bmatrix} = \begin{bmatrix} \boldsymbol{f} \\ \boldsymbol{0} \end{bmatrix} \tag{2.6}$$

where the superscript T denotes the transpose, $\boldsymbol{\alpha} = [\alpha_1, ..., \alpha_N]^T$, $\boldsymbol{\gamma} = [\gamma_1, ..., \gamma_M]^T$, $\boldsymbol{f} = [f(\boldsymbol{x_1}), ..., f(\boldsymbol{x_N})]^T$ and $\boldsymbol{0}$ is the matrix of all zeros of appropriate size. Sizes of the submatrices $\boldsymbol{\Phi}$ and $\boldsymbol{P}$ are $N \times N$ and $N \times M$ respectively. The matrix Φ is given by,

$$\boldsymbol{\Phi} = \begin{bmatrix} \phi\left(||\boldsymbol{x_1} - \boldsymbol{x_1}||_2\right) & \dots & \phi\left(||\boldsymbol{x_1} - \boldsymbol{x_q}||_2\right) \\ \vdots & \ddots & \vdots \\ \phi\left(||\boldsymbol{x_q} - \boldsymbol{x_1}||_2\right) & \dots & \phi\left(||\boldsymbol{x_q} - \boldsymbol{x_q}||_2\right) \end{bmatrix} \tag{2.7}$$

For a polynomial of maximum degree two, the matrix is given as:

$$\boldsymbol{P} = \begin{bmatrix} 1 & x_1 & y_1 & x_1^2 & x_1 y_1 & y_1^2 \\ \vdots & \vdots & \vdots & \vdots & \vdots & \vdots \\ 1 & x_q & y_q & x_q^2 & x_q y_q & y_q^2 \end{bmatrix} \tag{2.8}$$

Given the values of $\boldsymbol{f}$ at the scattered points, the values of $\boldsymbol{\alpha}$ and $\boldsymbol{\gamma}$ can be evaluated by solving eq. (2.6). The function $\boldsymbol{f}$ can then be evaluated at any arbitrary location $\boldsymbol{x}$ within the cloud. These relations can be implicitly used to determine the discrete values of $\boldsymbol{f}$ that satisfy a given governing equation at the discrete locations.

To determine the unknown variable, the governing differential equation is collocated at the scattered locations (Kansa, 1990a,b). The derivatives of the analytical interpolation

functions are equated to the right hand side of the governing partial differential equation at all the scattered points to get the discrete equation for $\boldsymbol{f}$. Let $\mathcal{L}$ denote the Laplacian (∇^2) operator. Then, we can write:

$$\mathcal{L}[f(\boldsymbol{x})] = \begin{bmatrix} \mathcal{L}[\boldsymbol{\Phi}] & \mathcal{L}[\boldsymbol{P}] \end{bmatrix} \begin{bmatrix} \boldsymbol{\alpha} \\ \boldsymbol{\gamma} \end{bmatrix} \tag{2.9}$$

$$= \begin{bmatrix} \mathcal{L}[\boldsymbol{\Phi}] & \mathcal{L}[\boldsymbol{P}] \end{bmatrix} \begin{bmatrix} \boldsymbol{D} \end{bmatrix}^{-1} \begin{bmatrix} \boldsymbol{f} \\ \boldsymbol{0} \end{bmatrix} = \begin{bmatrix} \boldsymbol{B}_1 & \boldsymbol{B}_2 \end{bmatrix} \begin{bmatrix} \boldsymbol{f} \\ \boldsymbol{0} \end{bmatrix} = \begin{bmatrix} \boldsymbol{B}_1 \end{bmatrix} \begin{bmatrix} \boldsymbol{f} \end{bmatrix} \tag{2.10}$$

The discrete coefficients for estimation of the Laplacian operator at each point are then combined in a global matrix of n rows (where n is the total number of scattered points), resulting in a set of linear equations given by,

$$\begin{bmatrix} \boldsymbol{A} \end{bmatrix} \begin{bmatrix} \boldsymbol{X} \end{bmatrix} = \begin{bmatrix} \boldsymbol{b} \end{bmatrix} \tag{2.11}$$

where $\boldsymbol{A}$ is a sparse matrix of the coefficients of size equal to the number of the scattered points and $\boldsymbol{b}$ is the vector of the source terms. $\boldsymbol{X}$ is the vector of all the unknown discrete values. The matrix $\boldsymbol{A}$ depends on the location of the scattered points relative to one another and can be stored at the start of the algorithm. The condition number for this matrix can be very high, leading to erroneous coefficients. This issue can be circumvented by shifting and scaling the positions of all the scattered points to a unit box as follows:

$$\boldsymbol{x_t} = \frac{\boldsymbol{x} - \min(\boldsymbol{x})}{\max(\boldsymbol{x}) - \min(\boldsymbol{x})} \qquad \boldsymbol{y_t} = \frac{\boldsymbol{y} - \min(\boldsymbol{y})}{\max(\boldsymbol{y}) - \min(\boldsymbol{y})} \tag{2.12}$$

where, $\boldsymbol{x}$ and $\boldsymbol{y}$ are the original co-ordinates of points in cloud and $\boldsymbol{x_t}$ and $\boldsymbol{y_t}$ are transformed co-ordinates. The RBF matrix A is first computed for the transformed co-ordinates and eq. (2.9) is solved. The coefficients for the global matrix are then scaled back to nullify the local non-dimensionalization so as to not impace the derivative values. At each discrete point, the computation of the $\boldsymbol{A}$ matrix requires a solution of a full matrix, but since each point is independent, these coefficients can be computed in parallel. Further economies can be gained by considering groups of points as one cluster and using the same $\boldsymbol{D}$ matrix for

points in the cluster (Shankar, 2017).

2.2 Multilvel procedure and RBF interpolation

Multilevel methods consist primarily of four different components. The first is generation of coarse levels for solving the equations to obtain corrections to the unknown variable. In structured grids, coarse levels can be obtained by picking alternative points from the fine level, thus doubling the grid spacing across all dimensions. Another alternative is to progressively agglomerate the finite volumes on the finest level. However, for meshless methods, the coarser levels are generated independent of the finest level. The average spacing in the coarser levels is higher, thus leading to fewer scattered points. The second component is the relaxation operator used to solve the differential equation at any level. The relaxation scheme can range from points solvers such as damped Jacobi and SOR to more powerful Krylov subspace solvers such as conjugate gradient, Chebyshev, BiCGSTAB and GMRES (Saad and Schultz, 1986). The purpose of the relaxation scheme is to anhilate the high frequency components of the errors and the number of relaxations at any levels can be fixed or adaptively changed based on convergence. The third component is the interpolation between the finer and coarser levels, to restrict residuals and prolongate coarse grid corrections. In structured grids, the restriction and prolongation can be obtained easily by using weighter bilinear or trilinear interpolation. However, since the scattered points for the meshless methods are arbitrarily spaced, the interpolation operators have to be constructed in different manner. Finally, the fourth component is the cycling strategy which defines the sequences in which the finer and coarser levels need to be visited. The details of the above steps for a meshless multilevel scheme are given below.

2.2.1 Generation of Coarse Level Point Sets

As mentioned above, we need to generate coarser levels of scattered points independent of the finest level. Thus, we will use the same procedure for grid generation for all levels, by making use of a finite element based mesh generator, but getting rid of all the elements and faces while preserving only the coordinated of the vertices. The quality of the grid characterized

by the slenderness of the elements does not explicitly affect the discretization accuracy as there is no explicit connectivity between points. However, decreasing average point spacings and thus increasing the total number of scattered points leads to a more accurate solution. In this thesis, we use Gmsh (Geuzaine and Remacle, 2009), an open-source finite element grid generator, to generate the scattered points at all levels.

2.2.2 Relaxation Operator

The coefficient matrix $\boldsymbol{A}$ in eq. (2.11) is stored in compressed sparse row (CSR) format using the Eigen library (Guennebaud et al., 2020) in C++. At Dirichlet boundaries, the interior equations are condensed with the substitution of boundary values. For Neumann boundaries, the cloud definition is altered to include only interior points. This is done so as to condense the boundary equations into the equations for the interior points, resulting in an implicit coupling of boundary and interior points. Thus, this new sparse matrix has the same size as that of the number of interior points. It is then re-ordered using the Reverse Cuthill-McGee (RCM) (Cuthill and McKee, 1969) algorithm to reduce the sparse bandwidth and increase computational efficiency. For the relaxation scheme, the SOR point solver with an over-relaxation of 1.4 is used. SOR has better convergence than damped Jacobi for most problems, although the Jacobi method is more amenable to parallelization. Point solvers are used in place of Krylov subspace solvers such as BiCGSTAB and GMRES to reduce the computational time, although they can also be used in multilevel methods.

2.2.3 Restriction and Prolongation Operators

For the correction based multilevel scheme, only the residuals of the Poisson equation need to be restricted to the coarser levels. The residuals on the finer level are calculated after a fixed number of relaxations as :

$$\boldsymbol{R^h} = \boldsymbol{b^h} - \boldsymbol{A}^h \boldsymbol{X^h} \tag{2.13}$$

where the superscript h refers to the set of points on the finer level and $\boldsymbol{R}$, $\boldsymbol{b}$, and $\boldsymbol{X}$ are vectors that denote the residual, the right-hand side, and the solution respectively. The residuals at the coarser set of points, denoted with superscript H are obtained by applying

the interpolation operator I_h^H which restricts the residuals as:

$$\boldsymbol{R}^H = \boldsymbol{I}_h^H \boldsymbol{R}^h \tag{2.14}$$

The interpolation operator $\boldsymbol{I}_h^H$ is constructed as follows. Given the coordinates of the coarse and fine sets of points, for the restriction operator we identify a cloud of closest fine level points for each one of the coarse set points. The number of fine level points for each coarse set point depends on the desired accuracy of the interpolation. Similarly for the prolongation operator, we define a cloud of closest coarse level points for each fine level point based on the desired accuracy. We use the same PHS-RBF interpolation procedure with appended polynomial as described earlier and a graphical representation of this interpolation operation is given in fig. 2.1.

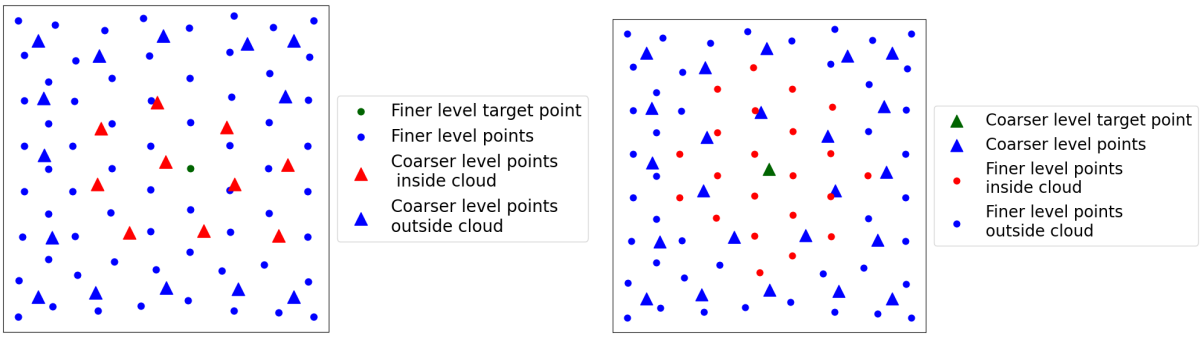

(a) Restriction from finer level to coarser level (b) Prolongation from coarser level to finer level

Figure 2.1: PHS-RBF interpolation between finer and coarser levels on a square geometry

The restriction of residuals from the finest level can be done at the same order of accuracy used for discretization. To construct the restriction operator, we start with the interpolation of fine level points over the selected cloud as:

$$f(\boldsymbol{x^h}) = \sum_{i=1}^{N^h} \alpha_i \phi(||\boldsymbol{x^h} - \boldsymbol{x_i^h}||_2) + \sum_{j=1}^{M^h} \gamma_j P_j(\boldsymbol{x^h}) \tag{2.15}$$

where N^h spans the cloud of fine points for a given coarse level point, and M^h represents the number of appended monomials. Collocation of the fine set values at the discrete points of interpolation gives the coefficients $\boldsymbol{\alpha}$ and $\boldsymbol{\gamma}$. Now the evaluation point for the function is set to the coarse level points. Thus, the resulting weights for each of the coarse level points is

stored in a sparse rectangular matrix, and this is done for each pair of fine and coarse levels to obtain the restriction operators. Similarly, the prolongation operators are obtained by switching the coarse and fine levels in the aforementioned procedure. The order of accuracy for the interpolation operators need not be as high as the discretization accuracy, in particular for the interpolation between intermediate levels. This can help save computational time by using a lower order polynomial in the PHS-RBF interpolation. By making use of the implicit boundary formulation, since the boundary equations are eliminated, the residual at the boundaries is set to zero.

A V-cycle multilevel scheme is used for this problem, which keeps restricting residuals after relaxation until the coarsest level is reached. At the coarsest level, a fixed number of relaxations are performed which constitutes the end of the down cycle. Once the coarse grid corrections are obtained at the coarsest level, they are prolongated and added to the values at the next finer level as follows:

$$\boldsymbol{X}^h = \boldsymbol{X}^h + \boldsymbol{I}_H^h \delta \boldsymbol{X}^H \tag{2.16}$$

The corrections at the Dirichlet boundaries are always zero, since the value is already known. However, for Neumann boundaries, the corrections have to be evaluated by making use of the interior coarse grid corrections and substituting them into the homogenous form of the Neumann boundary condition. A fixed number of relaxations are performed again after the prolongation of the corrections. The current restriction and prolongation operators are constructed using the geometric coordinates of the points and do not take into account the strength of coefficients as in AMG.

2.3 Applications to the fractional step method

The high-order discretization accuracy makes PHS-RBF meshless methods an attractive choice for solving practical fluid flow equation. Previous works in this direction have considered the Poisson equation (Bayona et al., 2017), scalar advection equation and the compressible Navier-Stokes equations (Barnett, 2015). The application of this method to in-

compressible flows has been however limited. In this work, we have developed a flow solver for incompressible flows using a time marching fractional step method (Harlow and Welch, 1965). The fractional step method first computes an intermediate velocity ($\hat{\boldsymbol{u}}$ and $\hat{\boldsymbol{v}}$) by ignoring the pressure gradient term in the momentum equations. Then, the divergence free constraint is enforced resulting in a pressure Poisson equation (PPE). The Neumann boundary conditions for pressure are obtained from the normal momentum equations at the boundaries. The two-step Adams-Bashforth method is used for time stepping the velocities. An overview of the fractional step method is given as follows:

$$\rho\frac{\hat{u}-u^n}{\Delta t} = 1.5(-\rho\boldsymbol{u}^n \bullet (\nabla u^n) + \mu\nabla^2 u^n) - 0.5(-\rho\boldsymbol{u}^{n-1} \bullet (\nabla u^{n-1}) + \mu\nabla^2 u^{n-1})) \tag{2.17}$$

$$\rho\frac{\hat{v}-v^n}{\Delta t} = 1.5(-\rho\boldsymbol{u}^n \bullet (\nabla v^n) + \mu\nabla^2 v^n) - 0.5(-\rho\boldsymbol{u}^{n-1} \bullet (\nabla v^{n-1}) + \mu\nabla^2 v^{n-1})) \tag{2.18}$$

$$\nabla \bullet (\nabla p) = \frac{\rho}{\Delta t}\left(\frac{\partial \hat{u}}{\partial x} + \frac{\partial \hat{v}}{\partial y}\right) \tag{2.19}$$

Here, the superscripts 'n' and 'n-1' refer to the previous time steps. As mentioned before, the two-step second order accurate Adams-Bashforth method is used for time stepping. The advection and diffusion terms are evaluated explicitly from the previous time steps. Implicit formulation is avoided as the divergence free constraint with implicit diffusion results in a Poisson equation for the potential function instead of pressure. This results in difficulties for the specification of Neumann boundary conditions and hence an explicit formulation is used to simplify matters at the cost of increased number of time steps.

Both the advection and diffusion terms are evaluated with the cloud-based interpolation scheme mentioned in section 2.1. Since the velocities at previous time steps are known, the advection and diffusion terms can be evaluated and the intermediate velocity can be updated at both the interior and boundary points. The boundary values for the velocities are specified by the Dirichlet boundary conditions. To satisfy the divergence free constraint, the pressure Poisson equation solved with the source term as the local divergence in the $\hat{\boldsymbol{u}}$ and $\hat{\boldsymbol{v}}$ velocity fields. At the boundaries, the normal momentum equation is used to specify

the Neumann boundary conditions as follows:

$$\nabla p \bullet \boldsymbol{N} = (-\rho(\boldsymbol{u} \bullet \nabla)\boldsymbol{u} + \mu\nabla^2\boldsymbol{u}) \bullet \boldsymbol{N} \tag{2.20}$$

where, $\boldsymbol{N}$ is the unit normal at the boundary points facing in the outward direction. Then, we use the multilevel procedure outlined section 2.2 to solve the Poisson equation to get the pressure field at all points. The regularization approach is used to take care of the null space arising due to all Neumann boundary conditions by setting the sum of pressures to be zero.

Finally, the velocities are corrected at the interior points by using the pressure field and the process is repeated until we reach steady state. The velocity correction equations are given below:

$$\rho\frac{u^{n+1} - \hat{u}}{\Delta t} = -\frac{\partial p}{\partial x} \tag{2.21}$$

$$\rho\frac{v^{n+1} - \hat{v}}{\Delta t} = -\frac{\partial p}{\partial y} \tag{2.22}$$

Chapter 3

Results for the Meshless Multilevel Algorithm Applied to the Poisson Equation

3.1 Problems considered

The convergence of the multilevel meshless algorithm is examined for the Poisson equation on three model 2D geometries. A manufactured solution is used to determine the discretization accuracy of the PHS-RBF meshfree method by substituting this solution into the Poisson equation to generate the source term. The following manufactured solution was considered:

$$T(x, y) = \cos(k\pi x)\cos(k\pi y) \tag{3.1}$$

which satisfies the Poisson equation,

$$\nabla^2 T(x, y) = -2\pi^2 k^2 \cos(k\pi x)\cos(k\pi y) \tag{3.2}$$

where k is the wavenumber of the manufactured solution. The following parameters were varied to check the multilevel convergence, 1) geometry; 2) wavenumber; 3) boundary condition (Dirichlet/Neumann); 4) number of scattered points on finest level; 5) degree of appended polynomial in the PHS-RBF discretization and 6) number of levels in the V-cycle. For Dirichlet conditions the exact value of the manufactured solution was specified on the boundary whereas for Neumann conditions the analytical derivatives of the manufactured so-

lution along the normal are prescribed. To save computational time, the degree of appended polynomial for the Poisson operator on all the coarser levels except the finest are set to three as this does not affect the discretization accuracy. The degree of appended polynomial is also set to three for all the restriction/prolongation matrices except the restriction from and the prolongation to the finest level for similar reasons.

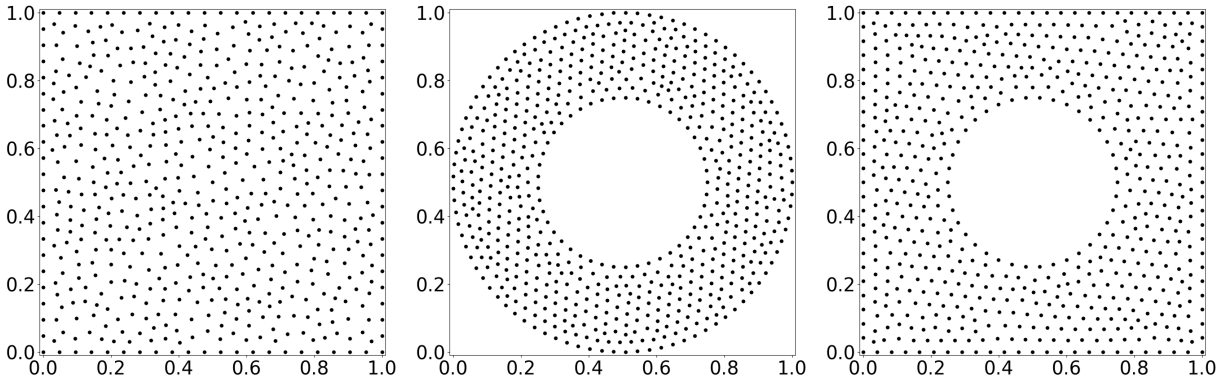

(a) Square (b) Circular annulus (c) Square-with-hole

Figure 3.1: Geometries considered and layout of discrete points

Figure 3.1 shows the three 2D geometries considered in this study. The scattered points shown were obtained from vertices of triangles generated by an open-source mesh generation software Gmsh (Geuzaine and Remacle, 2009). For each geometry, sets with different numbers of scattered points were obtained using the same software.

Geometry/Level	Square	Concentric annulus	Square-with-hole
1	98	90	89
2	169	188	176
3	607	650	640
4	2535	2581	2532
5	10023	10207	10197

Table 3.1: Numbers of points for each problem on different levels

Table 3.1 gives the numbers of points used for each problem on different levels. In addition to the three 2D model problems, the convergence of the multilevel algorithm is tested on a three dimensional cylinder. The length and diameter of the cylinder is set to one. Again,

SOR is used as the relaxation scheme with the number of relaxations fixed at five. The problem is tested for both Dirichlet and Neumann boundary conditions with varying degrees of appended polynomial between 3-6. The various levels considered for this problem in terms of number of scattered points is given in table 3.2.

Level	Number of points
1	1367
2	10,786
3	72,915
4	532,103

Table 3.2: Numbers of points on each level for 3D Cylinder

The discretization accuracy was computed as the L_1 norm of the difference between the converged discrete solution and the analytical solution defined as:

$$E = \frac{\sum_{i=1}^{n} |T_{PHS} - T_{exact}|_i}{\sum_{i=1}^{n} |T_{exact}|_i} \tag{3.3}$$

Convergence of the equations was monitored by the L_1 norm of the residuals defined as:

$$E = \frac{\sum_{i=1}^{n} |\nabla^2 T_{PHS} - RHS|_i}{\sum_{i=1}^{n} |RHS|_i} \tag{3.4}$$

The multilevel iterations were continued until the residual norm reached a value below 10^{-10}. The residuals are normalised with the norm of the vector of source terms. The number of SOR relaxations at any level before restricting the residuals and after prolongating the corrections are set to five. The over-relaxation factor for the SOR scheme is set to 1.4. The initial guess for all problems is set to a vector of zeros.

3.2 Dirichlet boundary conditions

For each of the three 2D geometries, the convergence was tested by varying the number of scattered points and the degree of appended polynomial. The calculations were also repeated for wavenumbers between 1 and 4. The degree of appended polynomial on the finest level

was varied between 3 and 6, and the number of scattered points was varied between around 625 points to around 10,000 points in steps of four.

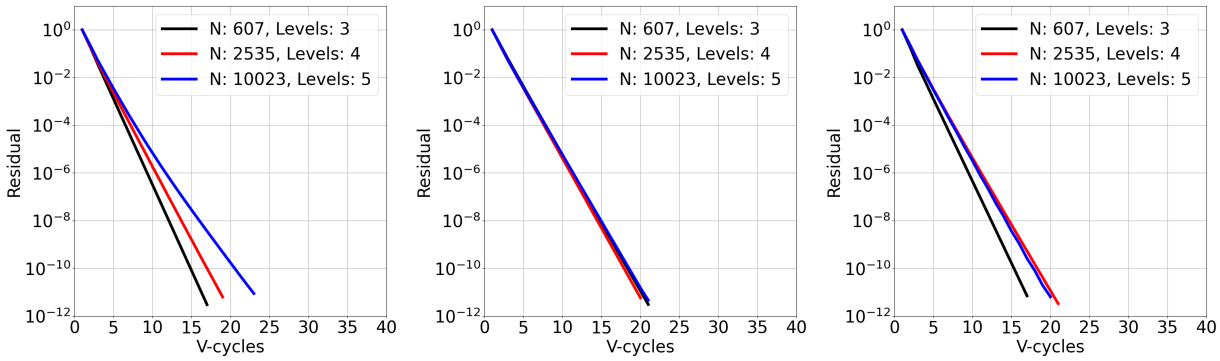

(a) Degree of appended polynomial = 3 (b) Degree of appended polynomial = 4 (c) Degree of appended polynomial = 6

Figure 3.2: Convergence of the residual on a square with Dirichlet boundary conditions

Figure 3.2 shows selected multilevel convergence histories for the square geometry using wavenumber $k = 1$ and three sets of points with polynomial degree of 3, 4, and 6. For each calculation, the coarsest level had 98 points. The number of points on all levels are given in table 3.1. Rapid convergence of the residual to a tolerance of 10^{-10} is observed in around 20 V-cycles, although the convergence is not completely independent of the number of scattered points. Increasing the degree of appended polynomial did not result in slower convergence for Dirichlet boundary conditions. Alternative cycling schemes such as W-cycle and full multigrid may improve convergence but are not explored in this study.

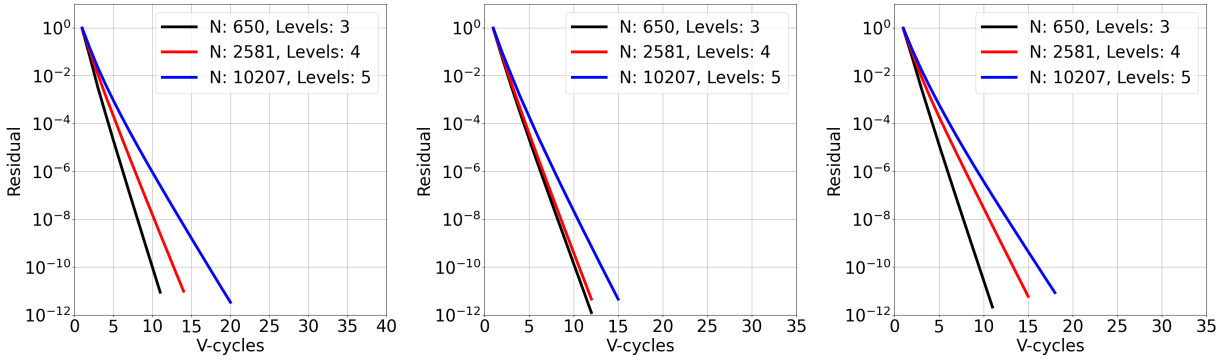

(a) Degree of appended polynomial = 3 (b) Degree of appended polynomial = 4 (c) Degree of appended polynomial = 6

Figure 3.3: Convergence of the residual on a concentric annulus with Dirichlet boundary conditions

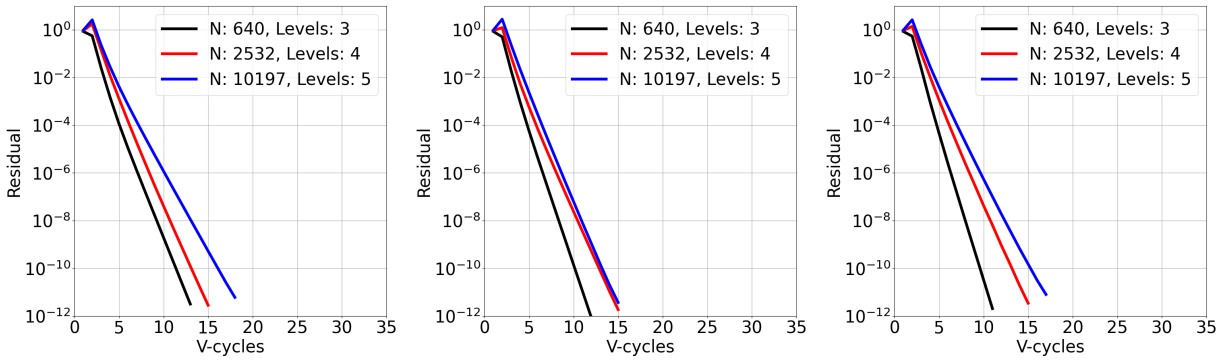

(a) Degree of appended polynomial = 3 (b) Degree of appended polynomial = 4 (c) Degree of appended polynomial = 6

Figure 3.4: Convergence of the residual on a square-with-hole geometry with Dirichlet boundary conditions

Figures 3.3 and 3.4 show similar convergence histories for the concentric annulus and the square-with-hole geometries respectively. The rate of convergence is very similar to that of the square case, taking about 15-20 V-cycles to reach the desired tolerance. The convergence for these cases are also not strictly independent of the number of scattered points, which means that the high-frequency errors on the finest level are not completely annihilated by 5 SOR sweeps.

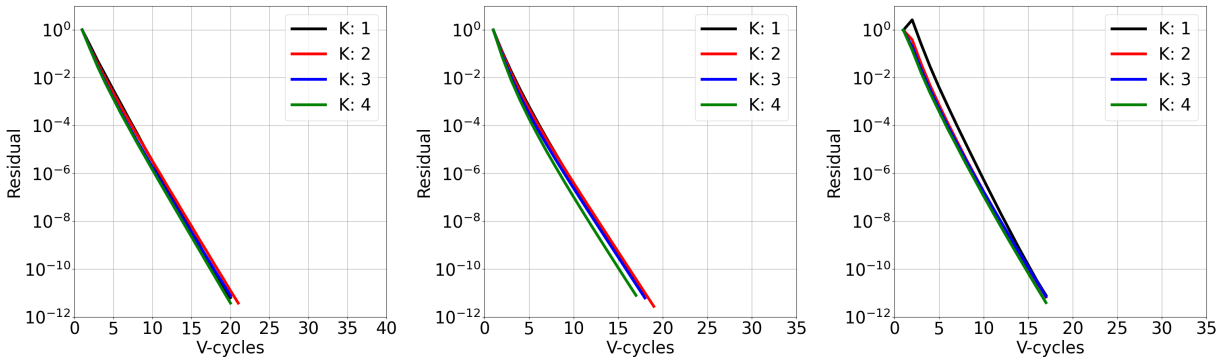

(a) Square, Degree of appended polynomial = 6 (b) Concentric annulus, Degree of appended polynomial = 6 (c) Square-with-hole, Degree of appended polynomial = 6

Figure 3.5: Effect of the wavenumber of the manufactured solution on multilevel convergence for finest level

Figure 3.5 shows the rates of convergence for different wavenumbers of the manufactured solution. The results presented correspond to a point set consisting of around $\sim 10,000$ points with an appended polynomial of degree 6. The coarsest set has ~ 90 points (5 levels).

For a single grid solver, a higher frequency manufactured solution will tend to converge faster due to the highly oscillatory nature of the errors. However, the benefit of using a multilevel scheme has ensured that all the wavenumbers converge at nearly the same rate. Thus, henceforth, the calculations are performed by fixing the wavenumber k at 1.

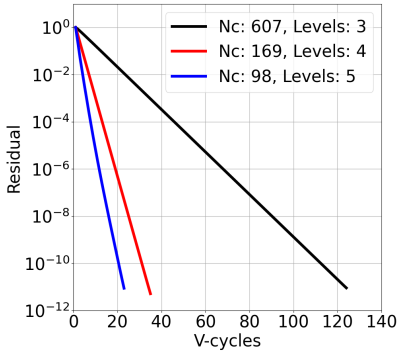

Figure 3.6: Effect of coarsest level on multilevel convergence

Figure 3.6 shows the rates of convergence for the square geometry with different degrees of coarsening. The finest level ws fixed at 10,023 points and the degree of appended polynomial was fixed at 3. The coarsest level was varied between 98 and 607 points from the levels tabulated in table 3.1. Decreasing the coarsest level in a multilevel scheme should lead to faster convergence as it leads to faster annihilation of the low frequency error components. This is manifested in our results by a factor of 5 reduction in the number of V-cycles from using five levels as opposed to three. The number of iterations for a single level relaxation scheme was significantly higher and hence is excluded here.

3.3 All-Neumann boundary conditions

Next, the case of Neumann boundary conditions on all faces is explored to examine convergence. Note that to eliminate the null space arising due to all-Neumann boundary conditions, the problem is regularised by introducing a constraint that fixes the sum of all values to zero. The solution matrix is thus modified by introducing a row and column with unity coefficients at the end as well as a zero on the source term. The Neumann boundary conditions are then implicitly substituted into the interior equations and the inhomogeneity is pushed to the right hand side accordingly.

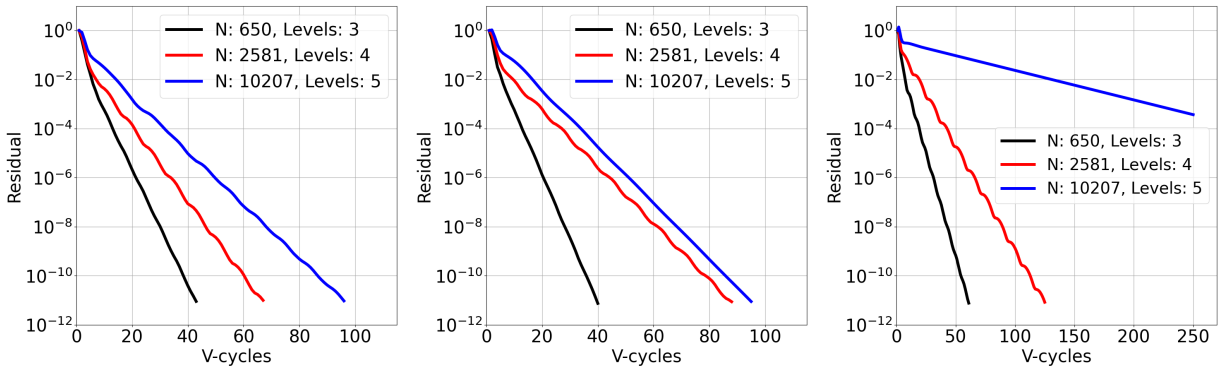

(a) Degree of appended polynomial = 3 (b) Degree of appended polynomial = 4 (c) Degree of appended polynomial = 5

Figure 3.7: Convergence of the residual on a concentric annulus with all-Neumann boundary conditions

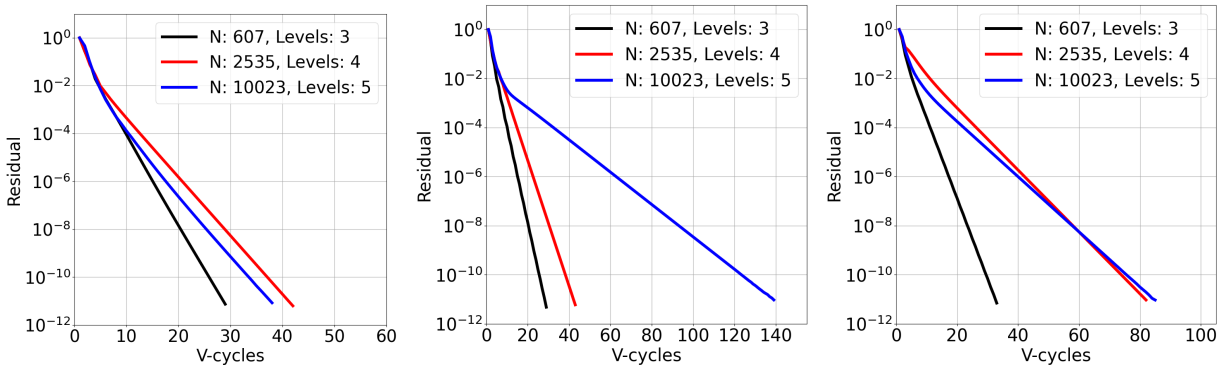

(a) Degree of appended polynomial = 3 (b) Degree of appended polynomial = 4 (c) Degree of appended polynomial = 5

Figure 3.8: Convergence of the residual on a square geometry with all-Neumann boundary conditions

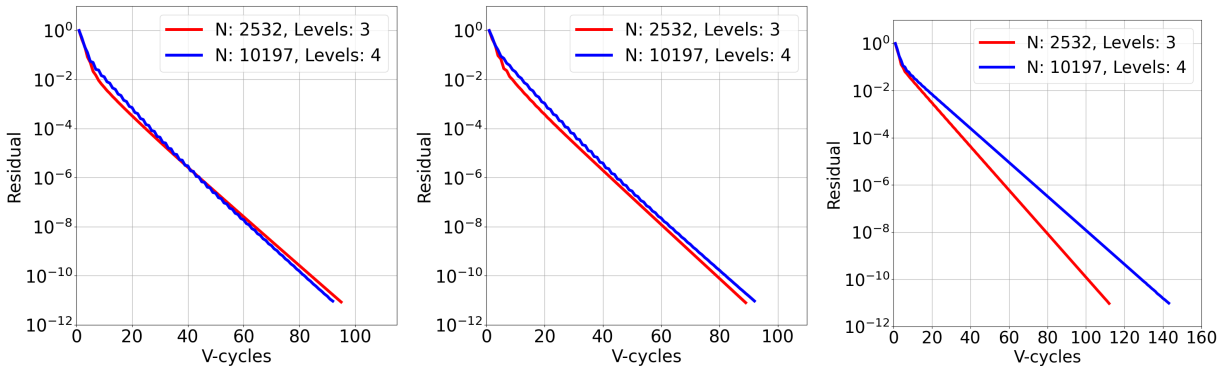

(a) Degree of appended polynomial = 3

(b) Degree of appended polynomial = 4

(c) Degree of appended polynomial = 5

Figure 3.9: Convergence of the residual on a square-with-hole geometry with all-Neumann boundary conditions (coarsest level = 176 points)

Figures 3.7 to 3.9 show the multilevel convergence for the three 2D problems with all Neumann boundary conditions. Five sweeps of SOR with an over-relxation factor of 1.4 is used as the smoother. It is observed that the convergence is significantly slower than that of the Dirichlet case. The convergence also seems to worsen significantly with increasing number of scattered points and increasing degree of appended polynomial for most of the cases. With the coarsest level fixed at 98 points, the square-with-hole case for high degree of appended polynomial (l = 5,6) diverged. It was found that limiting the coarsest level to 176 points gave better convergence in this case.

3.4 Multilevel preconditioned GMRES

The all-Neumann boundary condition is of particular importance in fluid flow solvers, for solving the pressure Poisson equation obtained by imposing the divergence free constraint in the momentum equations. Since the multilevel scheme mentioned before was seen to converge poorly for this case, we embedded this multilevel algorithm inside a Krylov Subspace Projector (KSP). The multilevel scheme was set as a preconditioner to the GMRES, a full projection method which works for unsymmetric matrices. The pseudo code for this algorithm is given below:

Let $x = 0$, $r = b$, $k = 0$, tol $= 10^{-10}$

while(true)

$k++$

Solve $M_g z = r$

if($k == 1$)

$p_k = z$

$w_k = Ap_k$

else

$p_k = z$

for $i = 1...k-1$

$p_k = p_k - [(w_i)^T(Az)/(w_i)^T(w_i)]$

$w_k = Ap_k$

$\alpha = (w_k)^T(Ar)/(w_k)^T(w_k)$

$x = x + \alpha p_k$

$r = r - \alpha w_k$

if ($(||r||/||b||) <$ tol)

break

Here, p_k's are mutually orthogonal in the A^TA norm, which is Symmetric Positive Definite (SPD) even if A is not SPD. Thus, the updated solution is the best fit in the space of the p_k's in the A^TA norm. Note that we have used modified Gram-Schmidt procedure to orthogonalize the search directions for better numerical stability. The solution to $M_g z = r$ applies one V-cycle of the multilevel operator M_g with the righthand side vector as r. The multilevel procedure starts with an initial vector of zero corrections and stores the result after one V-cycle in the vector z. This procedure was seen to be efficient and robust for all the pure Neumann boundary condition cases. Also, the number of V-cycles seemed to be fairly independent of the degree of appended polynomial.

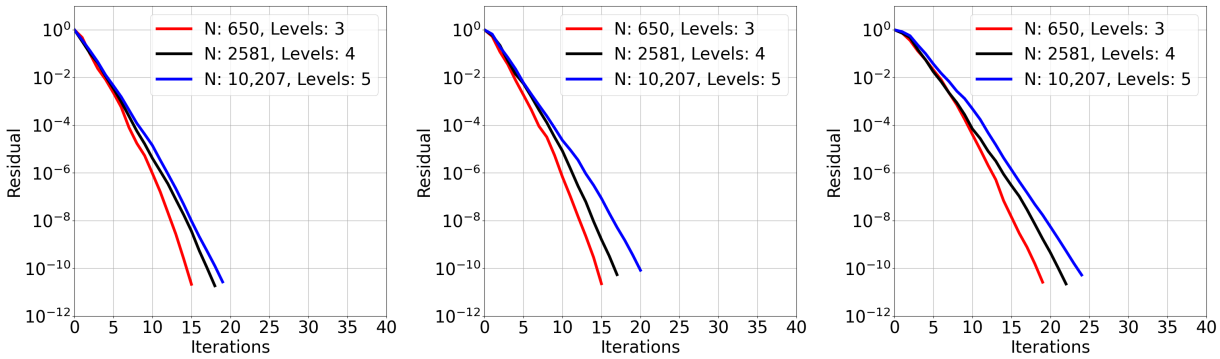

(a) Degree of appended polynomial = 4 (b) Degree of appended polynomial = 5 (c) Degree of appended polynomial = 6

Figure 3.10: Convergence of the GMRES-Multilevel algorithm for the concentric annulus with all-Neumann boundary conditions

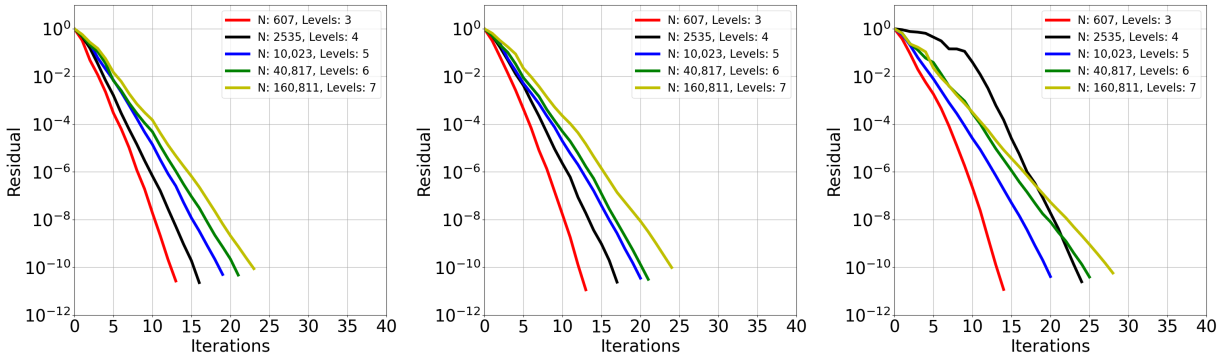

(a) Degree of appended polynomial = 4 (b) Degree of appended polynomial = 5 (c) Degree of appended polynomial = 6

Figure 3.11: Convergence of the GMRES-Multilevel algorithm for the square geometry with all-Neumann boundary conditions

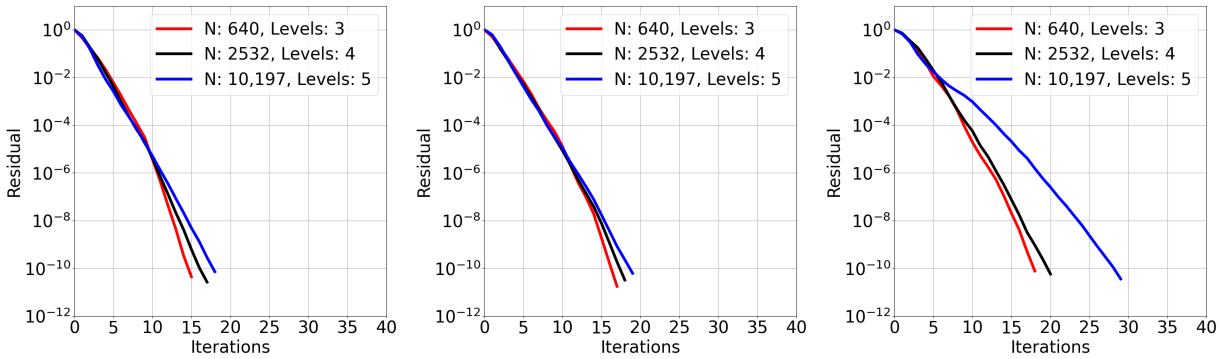

(a) Degree of appended polynomial = 4 (b) Degree of appended polynomial = 5 (c) Degree of appended polynomial = 6

Figure 3.12: Convergence of the GMRES-Multilevel algorithm for the square-with-hole geometry with all-Neumann boundary conditions

Figures 3.10 to 3.12 show the convergence trends for this modified algorithm for the three model 2D problems. Rapid convergence in less than 30 V-cycles is seen for all the cases, although the convergence is not strictly independent of the problem size. The convergence is also seen to worsen slightly for higher degree of appended polynomial due to a higher condition number of the sparse matrix. All further calculations in this thesis are thus performed using the multilevel preconditioned GMRES algorithm due to its superior results.

3.5 3D Dirichlet boundary conditions

The convergence of the multilevel preconditoned GMRES algorithm is tested on the 3D cylinder with Dirichlet boundary conditions imposed. The manufactured solution is prescribed on the boundaries with wavenumber $k = 1$ and five sweeps of SOR with an over-relaxation factor of 1.4 is used as the relaxation scheme. Level 1 (1367 points) in table 3.2 is fixed as the coarsest level and the finest level is varied between levels 2-4. The degree of appended polynomial is also varied between 3-6.

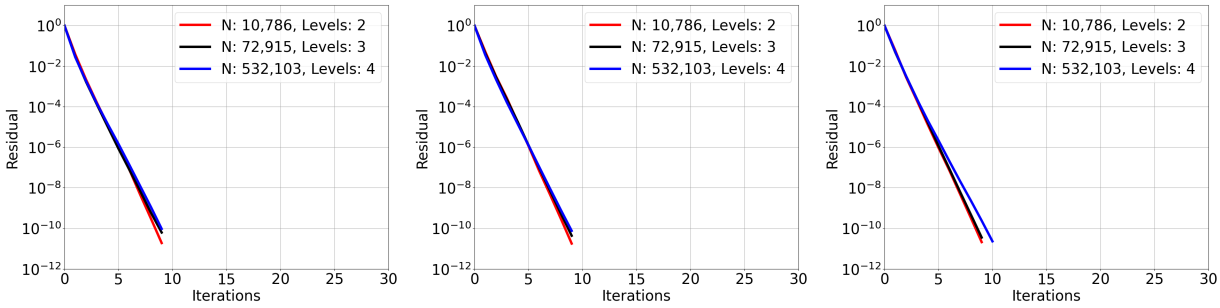

(a) Degree of appended polynomial = 4

(b) Degree of appended polynomial = 5

(c) Degree of appended polynomial = 6

Figure 3.13: Convergence of the GMRES-Multilevel algorithm for the 3D cylinder with Dirichlet boundary conditions

Figure 3.13 presents the convergence of the GMRES-Multilevel algorithm for the 3D Cylinder with degree of appended polynomial varying between 4-6. Rapid convergence to a tolerance of 10^{-10} in less than 10 V-cycles is observed for all cases. The number of V-cycles also remains constant with increasing number of scattered points and degree of appended polynomial, thus demonstrating the efficiency of the multigrid algorithm for this problem.

3.6 3D All-Neumann boundary conditions

For the all-Neumann boundary condition, SOR with an over-relaxation factor of 1.4, the residual diverges for all degrees of appended polynomial. Thus, to overcome this issue, successive under-relaxation is instead used as the relaxation scheme by setting ω to be less than 1 in the SOR algorithm. By varying ω, optimum convergence for $l = 3$ is observed when the under-relaxation factor is set to 0.75. However, for higher degrees of appended polynomials, the residual diverges for all values of ω. This can be attributed to the large bandwidth of the sparse matrix arising due to the increased number of monomials in 3D. To fix this issue, a defect correction approach is used for higher-order operators (l = 4,5,6) by using the lower-order ($l = 3$) operator as the iteration matrix in the relaxation scheme. The source term is then modified by adding the defect, which is the difference of the lower and higher order operators multiplied by the vector of values, arising due to using the lower-order operator, thus maintaining higher-order discretization accuracy.

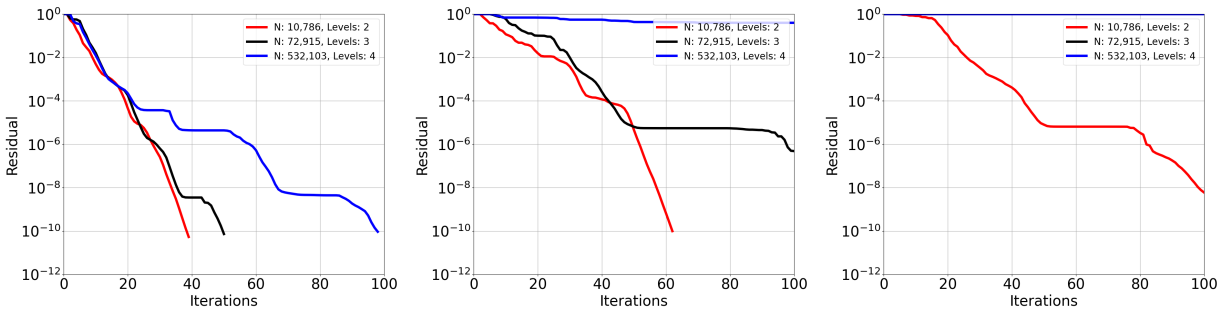

(a) Degree of appended polynomial = 3

(b) Degree of appended polynomial = 4

(c) Degree of appended polynomial = 5

Figure 3.14: Convergence of the GMRES-Multilevel algorithm for the 3D cylinder with Neumann boundary conditions

Figure 3.14 demonstrates the convergence for the GMRES-Multilevel algorithm on a 3D cylinder with Neumann boundary conditions. Although the defect correction approach fixes the divergence of the residual, it can be seen that the convergence becomes increasingly poor for higher degrees of appended polynomials. Also, increasing the number of scattered points results in significantly higher number of V-cycles for convergence, which indicates that the relaxation scheme used in this case is not ideal. Other relaxation schemes such as Chebyshev or block-SOR may lead to better convergence and will be explored in future studies.

3.7 Discretization errors

The order of accuracy of the PHS-RBF method varies exponentially with point spacing as per the degree of the appended polynomial. The discretization accuracy is demonstrated by plotting the difference between the manufactured solution for all the three 2D problems as well as the 3D cylinder. The PHS-RBF operator with degree of appended polynomial l usually demonstrates an $(l-1)$ order accuracy for the second derivative used in the Poisson operator.

The calculated errors for each case are plotted in fig. 3.15 for polynomial degree of 5 against an average spacing Δx defined as:

$$\Delta x = (Ar/n)^{0.5} \tag{3.5}$$

where Ar and n in eq. (3.5) refer to the area of the domain and number of points respectively.

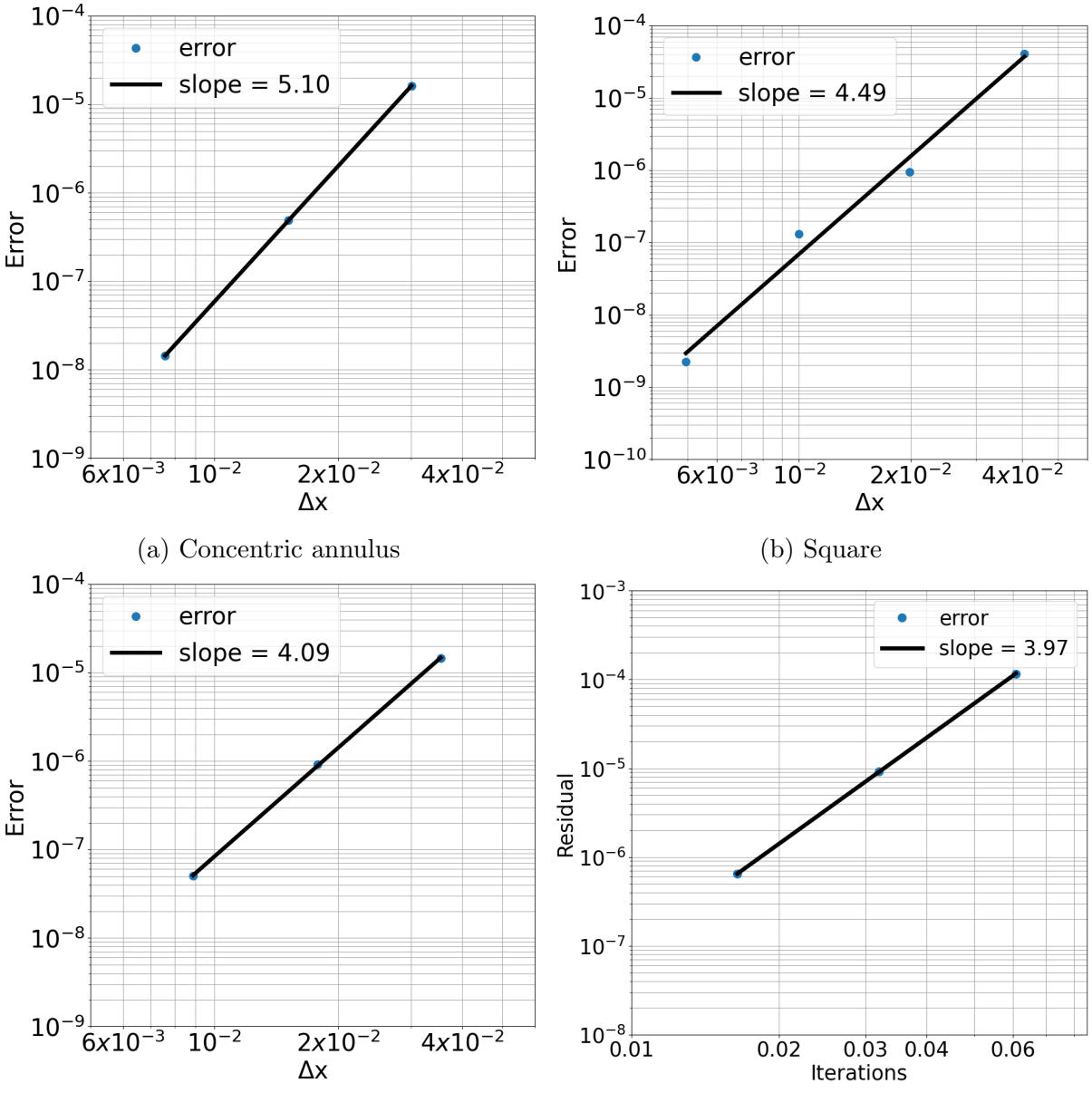

(a) Concentric annulus

(b) Square

(c) Square-with-hole

(d) 3D Cylinder

Figure 3.15: Discretization errors for various geometries with degree of appended polynomial of 5.

Figure 3.15 shows that the errors are following the expected trends. In addition, the polynomial degree can also be varied locally to get high-order accuracy in targeted regions.

Chapter 4

Results for the Meshless Fractional Step Algorithm

4.1 Problems considered

The GMRES-multilevel meshfree algorithm is now applied to the pressure Poisson equation in the fractional step algorithm. All-Neumann boundary conditions are used for pressure and the source term is calculated using the normal momentum equation to ensure high-order accuracy of the PHS-RBF discretization.The aforemtnioned algorithm is used to solve the Navier-Stokes equations for four fluid flow problems. The first problem considered is Kovasznay flow (Kovasznay, 1948) and the second problem is Couette flow between two cylinders with the inner cylinder rotating at a constant speed. Both these problems have analytical solutions that satisfy the Navier-Stokes equations which can be used to verify the high-order accuracy of the meshfree method. Once this is done, we apply this algorithm to two model flows: flow in an an eccentric annulus with a rotating inner cylinder and flow arising due to a rotating cylinder inside an ellipse. Since these two model problems have no analytical solutions, the convergence of the discretization error is verified by comparing the numerical solution to the numerical solution obtained with a large number of scattered points and a high degree of appended polynomial (6). As before, the vertices of a finite element grid generated by Gmsh (Geuzaine and Remacle, 2009) are used as scattered points. The residual tolerance for the meshfree multilevel preconditioned GMRES algorithm for the solution of the pressure Poisson equation is set at 10^{-10} and the steady state tolerance is set at 10^{-12}. Adams-Bashforth method is used for timestepping the solution, thus maintaining

the second order accuracy in time. The degree of appended polynomial is varied between 3-6 for each of these problems.

4.2 Kovasznay flow

The first problem considered for demonstrating the algorithm is laminar flow behind a two dimensional grid, otherwise known as Kovasznay flow (Kovasznay, 1948). The analytical solution to Kovasznay flow is given in terms of a non-dimensional parameter λ, which is a function of Reynolds number:

$$\lambda = \frac{Re}{2} - \left(\frac{Re^2}{4} + 4\pi^2 \right)^{0.5} \tag{4.1}$$

The X and Y components of velocity and pressure denoted by u, v and p respectively, are given as :

$$\begin{aligned} u &= 1 - \exp(\lambda x)\cos(2\pi y) \\ v &= \lambda \exp(\lambda x)\sin(2\pi y)/(2\pi) \\ p &= p_0 - (\exp(2\lambda x)/2) \end{aligned} \tag{4.2}$$

A unit square with X and Y values ranging from -0.5 to 0.5 is considered with the flow being periodic along the Y direction. Dirichlet boundary conditions for u and v are prescribed from the analytical solutions. The intermediate velocities $\hat{u}$ and $\hat{v}$ are calculated at both interior and boundary points, and the Neumann boundary conditions for the pressure Poisson equation are determined using the normal momentum equations. The solution is timestepped to steady state, ensuring the convergence of the residuals to the specified tolerance for the Poisson equation at each timestep. The initial guess is set to a vector of zeros for both the velocities as well as pressure and the Reynolds number is set to 40. Three sets of points are considered with 1053, 5031 and 10665 points. As an example, the distribution with 1053 points is plotted in fig. 4.1a. The streamlines and contours of pressure are shown in fig. 4.1b.

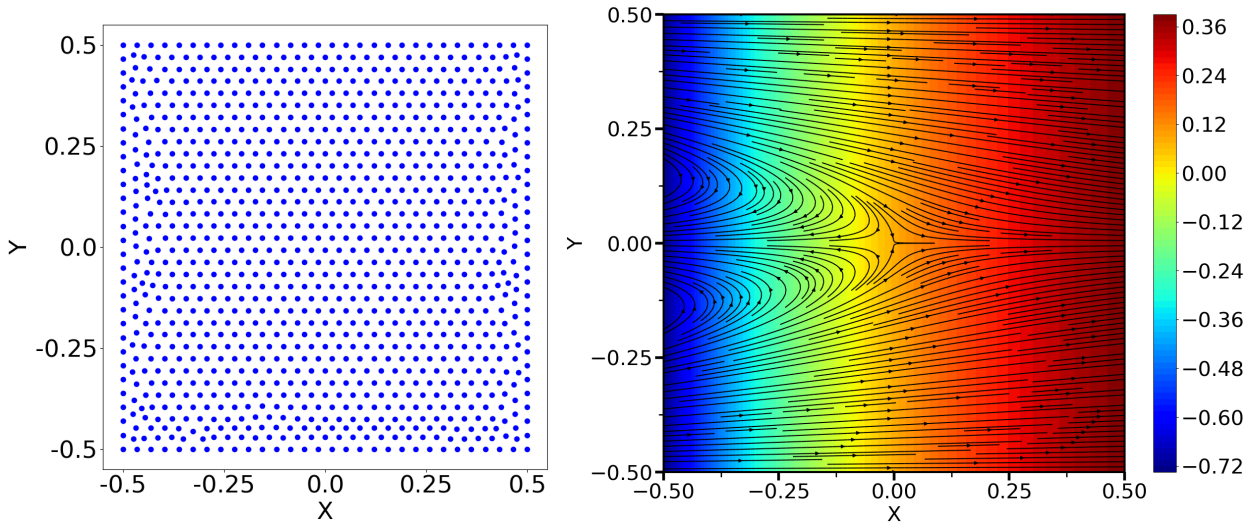

(a) Distribution of 1053 Points

(b) Streamlines Superposed on Pressure Contours

Figure 4.1: Kovasznay Flow

The discretization accuracy of pressure and velocity components is determined by calculating the relative error in the L_1 norm from the analytical values. The discretiztion errors are plotted against the grid spacing Δx in fig. 4.2. The grid spacing is defined as: $\Delta x = \sqrt{(\text{flow area})/n_p}$ where, n_p is the total number of points. The L_1 norm of the divergence of the velocity field is also plotted alongside the errors for both the velocities and pressure. For each polynomial degree, a best fit line is fitted to determine the order of convergence. It is seen that the polynomial of degree l is at least $(l-1)$ order accurate.

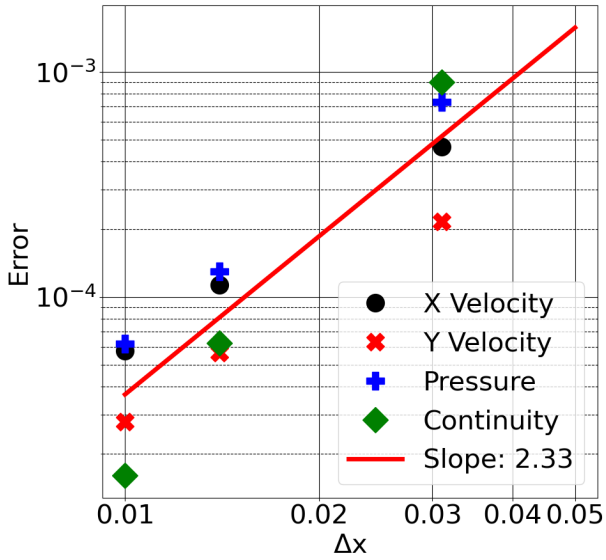

(a) Degree of Appended Polynomial: 3

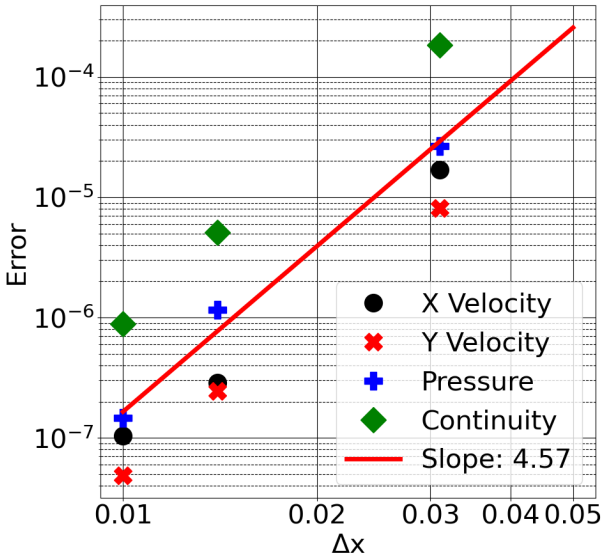

(b) Degree of Appended Polynomial: 4

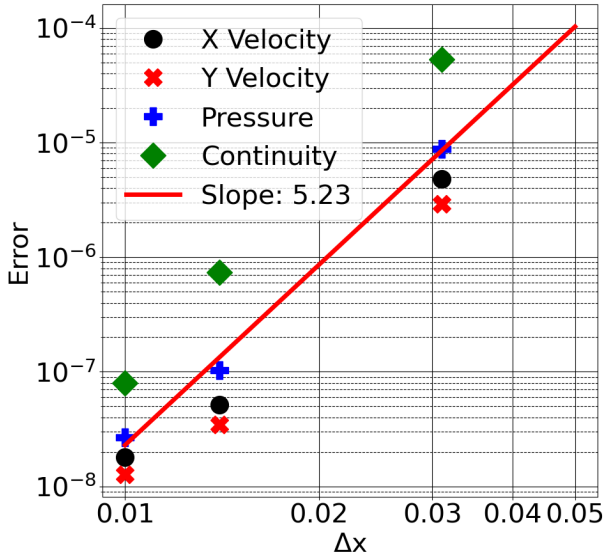

(c) Degree of Appended Polynomial: 5

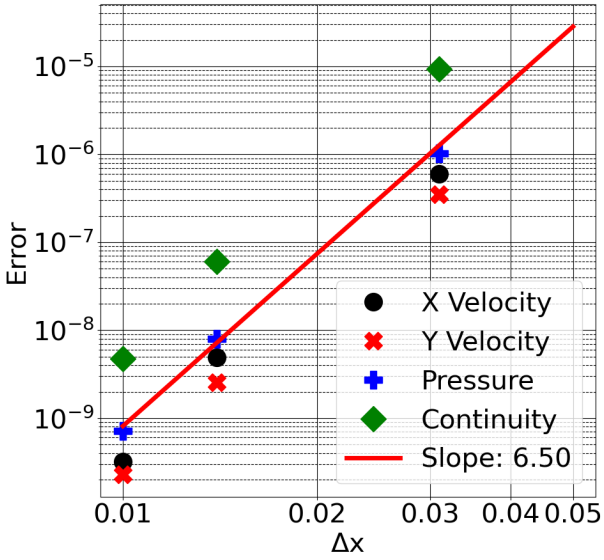

(d) Degree of Appended Polynomial: 6

Figure 4.2: Errors for Kovasznay Flow

4.3 Concentric cylindrical Couette flow

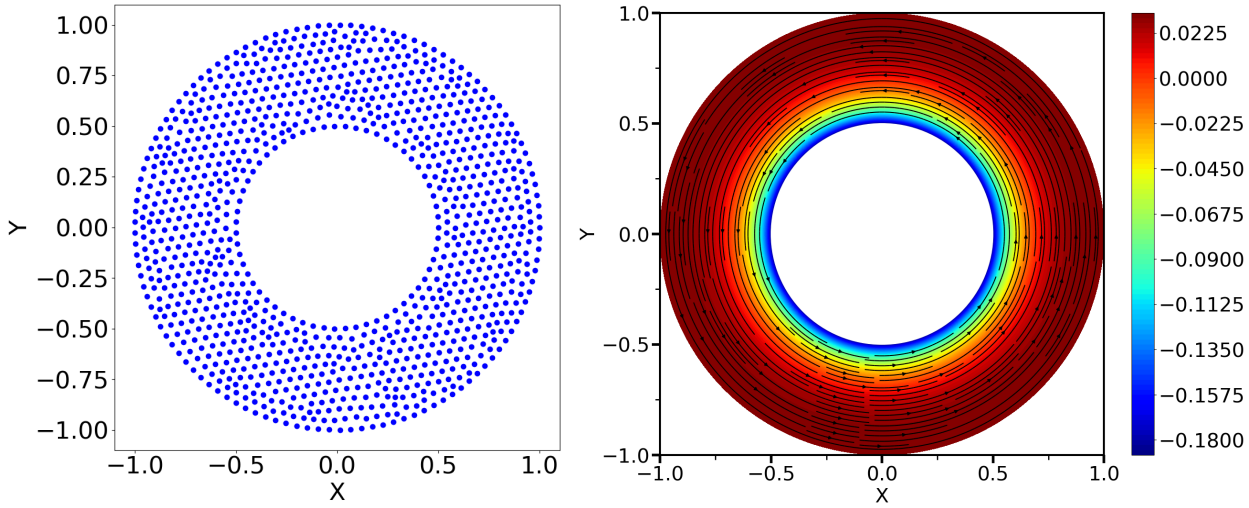

(a) Distribution of 1073 Points (b) Streamlines Superposed on Pressure Contours

Figure 4.3: Cylindrical Couette Flow

The cylindrical Couette flow is a one-dimensional solution to the Navier-Stokes equations in polar coordinates along the tangential direction. However, our solver uses the Cartesian coordinate system to generate the Navier-Stokes equations, resulting in a two-dimensional flow along X and Y axes. The low rotational Reynolds number inhibits the formation of longitudinal Taylor vortices. The inner cylinder rotates with angular velocity ω while the outer cylinder remains stationary. The no slip and no penetration boundary conditions result in a steady, laminar fluid flow with the analytical solution of the tangential velocity (v_θ in terms of the radial coordinate (r) given as:

$$v_\theta(r) = r_1\omega\frac{r_1 r_2}{r_2^2 - r_1^2}\left(\frac{r_2}{r} - \frac{r}{r_2}\right) \tag{4.3}$$

where r_2 and r_1 denote the radii of the outer and inner cylinders respectively. The Reynolds number is based on inner cylinder's diameter and its tangential velocity. The solution to the Couette flow however is independent of the Reynolds number, thus an arbitrary value of 100 is used. The inner and outer radii are set as 0.5 and 1 respectively, resulting in an aspect ratio $A = (r_2 - r_1)/r_1$ of unity. To investigate the convergence characteristics, three different sets of points are considered: 1073, 5630 and 10738. The momentum equations are used

to determine $\hat{u}$ and $\hat{v}$ as before and the normal momentum equations are used to generate the Neumann boundary conditions for pressure. The pressure Poisson equation is made to converge to the desired tolerance at each timestep using the GMRES-multilevel algorithm and the solution is marched to steady state. The relative errors in the L_1 norm between the analytical and numerical solutions as well as the divergence of the velocity field are plotted in fig. 4.4. For this problem, the order of accuracy is seen to be at least l, where l is the degree of appended polynomial.

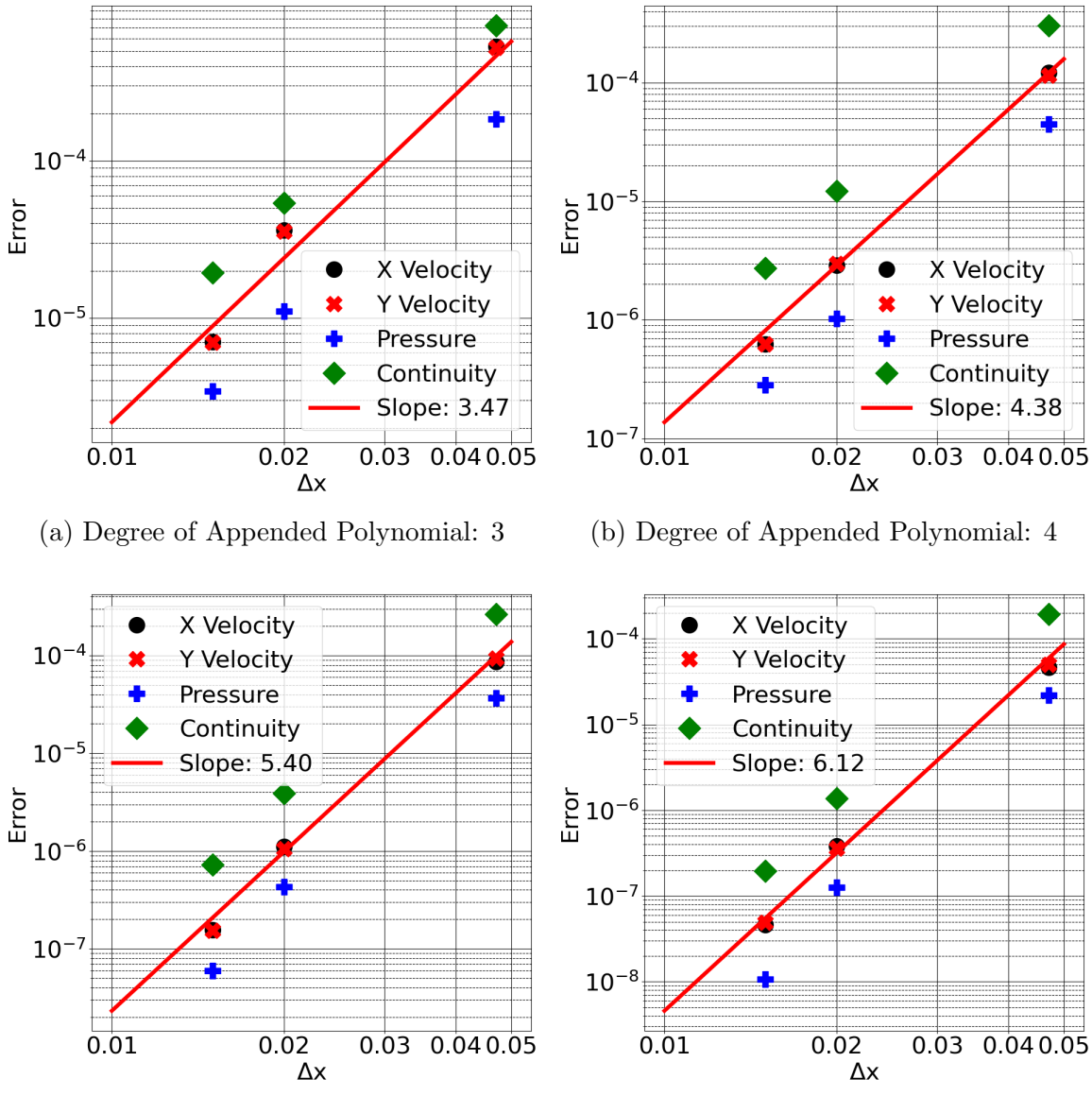

(a) Degree of Appended Polynomial: 3

(b) Degree of Appended Polynomial: 4

(c) Degree of Appended Polynomial: 5

(d) Degree of Appended Polynomial: 6

Figure 4.4: Errors for Cylindrical Couette Flow

4.4 Eccentric cylindrical Couette flow

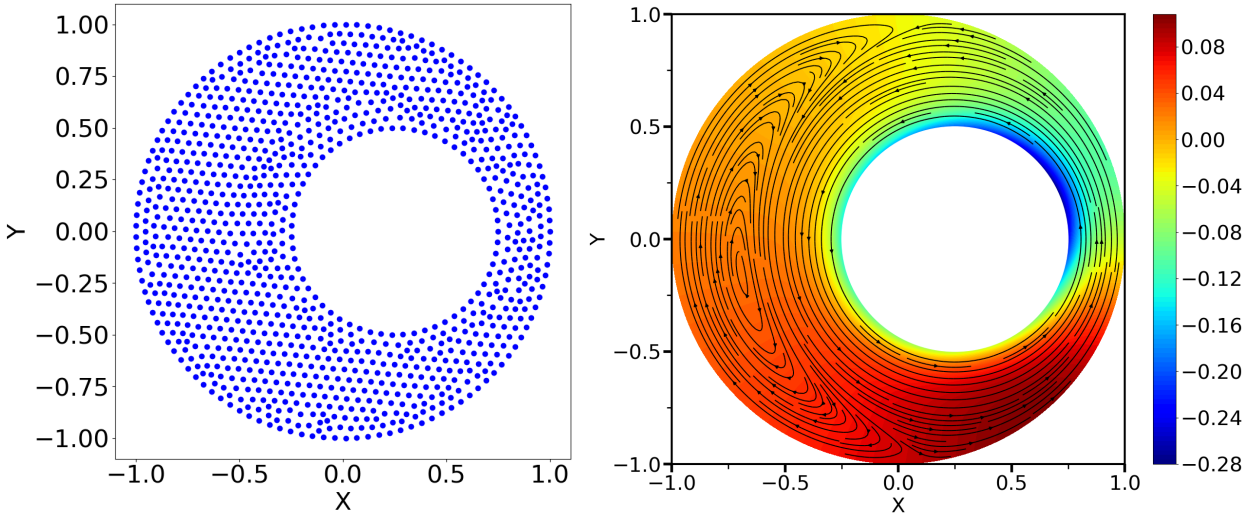

(a) Distribution of 1076 Points (b) Streamlines Superposed on Pressure Contours

Figure 4.5: Eccentric Cylindrical Couette Flow

The third problem considered is the flow between two cylinders such that their axes are no longer coincident. The aspect ratio $A = (r_2 - r_1)/r_1$ and eccentricity $e = d/(r_2 - r_1)$ (where d is the perpendicular distance between axes of the cylinders) are fixed at 1 and 0.5 respectively, with $r_2 = 1$ and $r_1 = 0.5$. The Reynolds number based on the tangential velocity and d is set to 50. Varying numbers of points, as in the case of concentric cylinder, are considered (1076, 5014 and 10533). Figure 4.5a shows an example of point distribution. The contours of the pressure superposed with streamlines are plotted in fig. 4.5b. These are in agreement with a previous study performed with a ghost fluid Lattice Boltzmann method (Tiwari and Vanka, 2012).

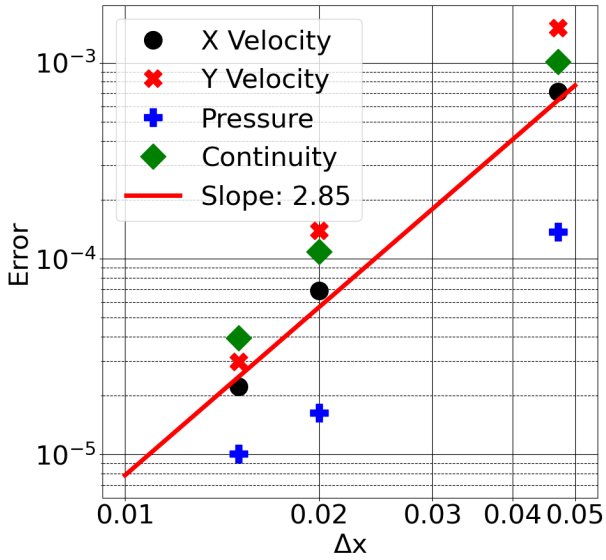

(a) Degree of Appended Polynomial: 3

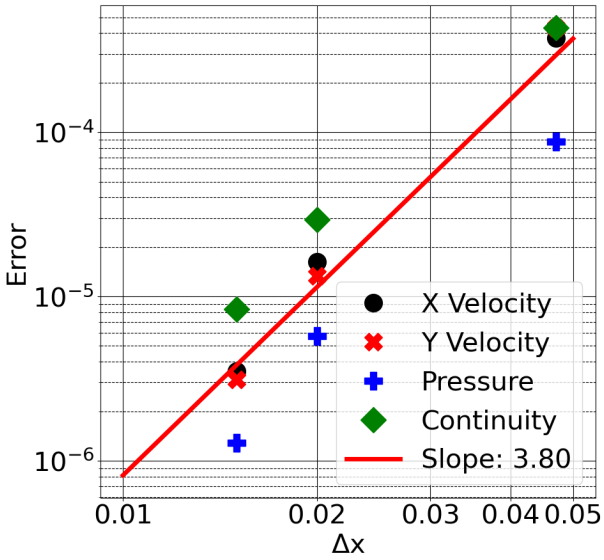

(b) Degree of Appended Polynomial: 4

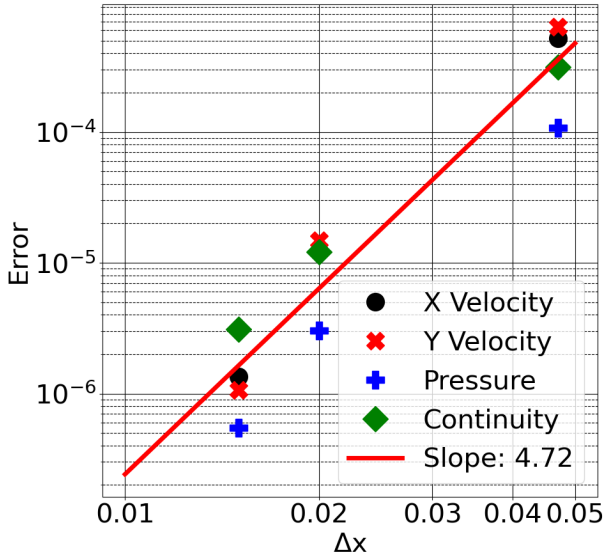

(c) Degree of Appended Polynomial: 5

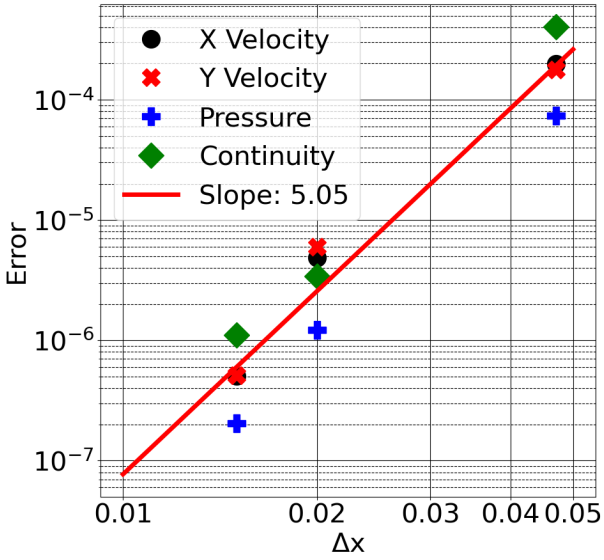

(d) Degree of Appended Polynomial: 6

Figure 4.6: Errors for Eccentric Cylindrical Couette Flow

Due to the absence of an analytical solution, a numerical solution is generated using 55419 points and degree of appended polynomial 6, which is used to generate the discretization errors in fig. 4.6. The discretization error is at least $(l-1)$ order accurate where l is the degree of appended polynomial. The solution is also interpolated to 15 points distributed uniformly along $X = -0.35$ using PHS-RBF interpolation with polynomial degree 6. The solutions are documented in table 4.1

X	Y	u	v	p
-0.35	-8.0000000E-01	-1.9079592E-02	4.7313446E-03	4.9115286E-02
-0.35	-6.8571429E-01	8.1661301E-03	-1.9183109E-02	4.5560404E-02
-0.35	-5.7142857E-01	6.1684959E-02	-7.5648774E-02	4.0809071E-02
-0.35	-4.5714286E-01	1.2197777E-01	-1.6810504E-01	3.3351733E-02
-0.35	-3.4285714E-01	1.6431517E-01	-2.9251677E-01	2.0851835E-02
-0.35	-2.2857143E-01	1.6299774E-01	-4.3025881E-01	2.5791952E-03
-0.35	-1.1428571E-01	1.0359107E-01	-5.4349940E-01	-1.7126709E-02
-0.35	2.7755576E-17	6.7240764E-04	-5.8731376E-01	-2.9612243E-02
-0.35	1.1428571E-01	-1.0148266E-01	-5.4042011E-01	-3.0062418E-02
-0.35	2.2857143E-01	-1.5882169E-01	-4.2423074E-01	-2.3165751E-02
-0.35	3.4285714E-01	-1.5830580E-01	-2.8515341E-01	-1.7072929E-02
-0.35	4.5714286E-01	-1.1702532E-01	-1.6228223E-01	-1.5428133E-02
-0.35	5.7142857E-01	-6.1749566E-02	-7.3639191E-02	-1.7157194E-02
-0.35	6.8571429E-01	-1.4637270E-02	-2.1045138E-02	-2.0009898E-02
-0.35	8.0000000E-01	1.0178600E-02	1.4208480E-03	-2.2632250E-02

Table 4.1: Reference Values for Eccentric Cylindrical Couette Flow

4.5 Flow in an elliptic annulus with rotating inner cylinder

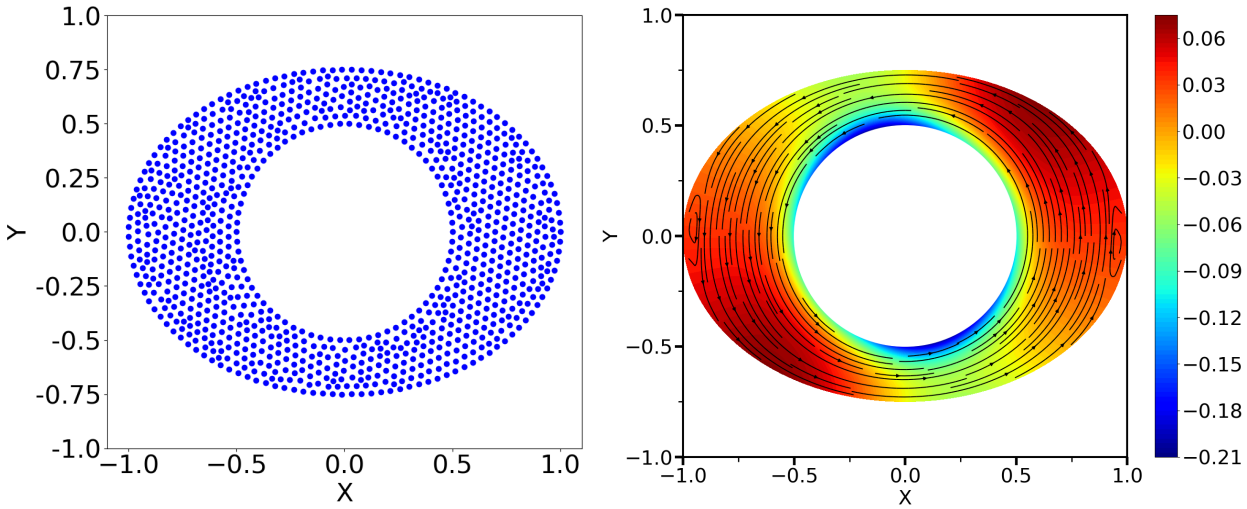

(a) Distribution of 1036 Points (b) Streamlines Superposed on Pressure Contours

Figure 4.7: Flow in an Elliptical Annulus with Rotating Inner Cylinder

The last problem considered is the flow in an annulus formed between an elliptic enclosure and a rotating inner cylinder, with coincident axes. The flow is similar to that of Couette flow, except for the fact that the outer cylinder is now replaced with an ellipse. Three sets of points are considered (1036, 5057 and 10440) and the Reynolds number based on the inner cylinder diameter is set to 50. Figure 4.7b shows the contours of the pressure and streamlines from the finest set of points.

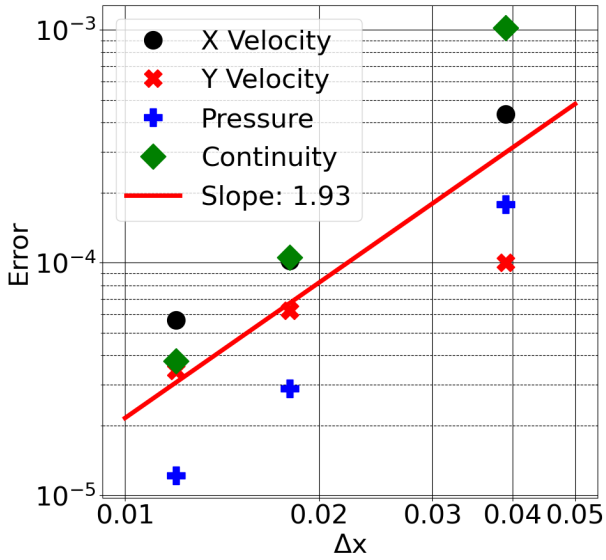

(a) Degree of Appended Polynomial: 3

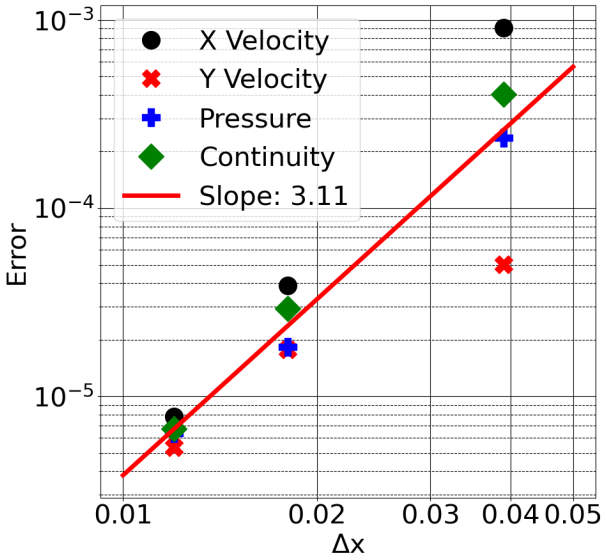

(b) Degree of Appended Polynomial: 4

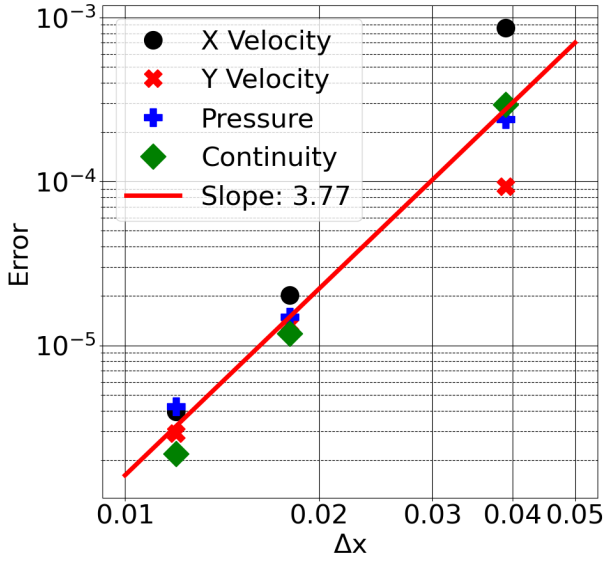

(c) Degree of Appended Polynomial: 5

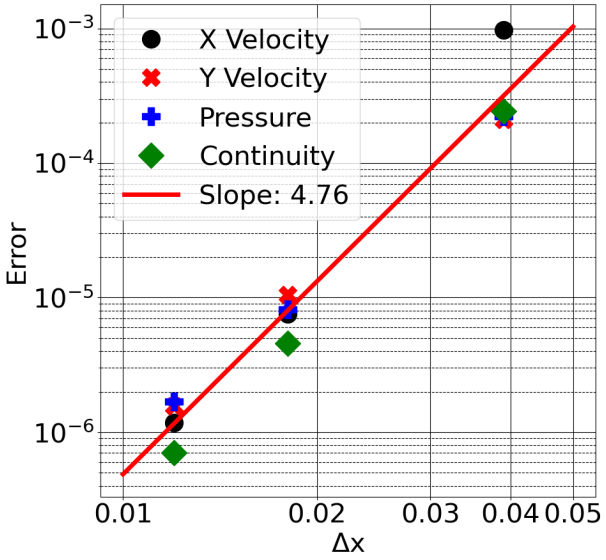

(d) Degree of Appended Polynomial: 6

Figure 4.8: Errors for Flow in an Elliptical Annulus with Rotating Inner Cylinder

As in section 4.4, due to the absence of an analytical solution, a numerical solution with 51412 points and appended polynomial degree 6 is used to generate the discretization errors in fig. 4.7. The order of accuracy for a degree l appended polynomial degree is approximately $(l-1)$. The reference values for both the velocity components and the pressure are generated by interpolating the finest level numerical solution to 15 points along $X = 0$. PHS-RBF interpolation is used for this purpose and the reference solution is given in table 4.2.

X	Y	u	v	p
0.00	5.0000000E-01	-1.0000000E+00	1.2833611E-14	-1.1921286E-01
0.00	5.1785714E-01	-9.4873251E-01	1.5998650E-05	-8.5927834E-02
0.00	5.3571429E-01	-8.9293824E-01	-2.1156478E-04	-5.7615108E-02
0.00	5.5357143E-01	-8.3368481E-01	-8.0766410E-04	-3.3924495E-02
0.00	5.7142857E-01	-7.7184033E-01	-1.6753742E-03	-1.4429810E-02
0.00	5.8928571E-01	-7.0790039E-01	-2.6278077E-03	1.3266544E-03
0.00	6.0714286E-01	-6.4198095E-01	-3.4644281E-03	1.3800200E-02
0.00	6.2500000E-01	-5.7389110E-01	-4.0154090E-03	2.3424082E-02
0.00	6.4285714E-01	-5.0323668E-01	-4.1680020E-03	3.0601974E-02
0.00	6.6071429E-01	-4.2952646E-01	-3.8821536E-03	3.5708587E-02
0.00	6.7857143E-01	-3.5226288E-01	-3.1984837E-03	3.9094469E-02
0.00	6.9642857E-01	-2.7100522E-01	-2.2395268E-03	4.1091713E-02
0.00	7.1428571E-01	-1.8539674E-01	-1.2041977E-03	4.2018226E-02
0.00	7.3214286E-01	-9.5151425E-02	-3.5528821E-04	4.2179153E-02
0.00	7.5000000E-01	-9.5963561E-13	1.4881676E-13	4.1865046E-02

Table 4.2: Reference Values for Flow in an Elliptical Annulus with Rotating Inner Cylinder

Chapter 5

Conclusion

In this thesis, a multilevel algorithm to solve the Poisson equation resulting from the meshless discretization in a complex domain is presented. PHS-RBFs with appended polynomials are used to generate the meshless operator as they do not suffer from stagnation issues due to the absence of a shape parameter and SOR is used as the relaxations scheme. The multilevel algorithm uses independent point sets and restriction/prolongation matrices which are generated using PHS-RBF interpolation. First, the algorithm was applied to three model geometries in 2D. The algorithm showed rapid convergence for Dirichlet boundary conditions for large number of scattered points and high appended polynomial degrees. However, for the case of all-Neumann boundary condition, the convergence seemed to be inferior and significantly worsened with increasing number of points as well as polynomial degrees. To overcome this issue, the multilevel algorithm was used as a preconditioner to GMRES. The multilevel preconditioned GMRES demonstrated rapid and robust convergence for all three model problems in 2D for both Dirichlet and all-Neumann boundary conditions. Furthermore, the convergence of the multilevel-GMRES algorithm was investigated for a 3D cylinder with both Dirichlet and all-Neumann boundary conditions. While rapid convergence was obeserved for Dirichlet boundary conditions, the convergence for all-Neumann boundary conditions was unsatisfactory, in particular for higher number of scattered points. The poor convergence can be attributed to the very large bandwidth arising in 3D all-Neumann problems from the implicit substitution of boundary equations, resulting in the divergence of the SOR scheme.

The multilevel-GMRES algorithm was then applied to the pressure Poisson equation arising in the fractional step method for four 2D fluid flow problems. All-Neumann boundary

conditions for the pressure Poisson were generated from the normal momentum equations to maintain high-order accuracy. The high-order discretization accuracy was verified using two model problems with analytical solutions, namely Kovasznay flow and concentric circular Couette flow. Then, the algorithm was applied to generate reference solutions to two model problems, the eccentric circular Couette flow and the flow in an elliptic annulus due to a rotating inner cylinder. The convergence in these cases was demonstrated by using a numerical solution with large number of scattered points and high degree of appended polynomial.

Future efforts will be directed towards improving the convergence for all-Neumann boundary conditions in three dimensions by using a better relaxation scheme such as block-SOR or Chebyshev iteration. This will facilitate the solution of the pressure Poisson equation in 3D fluid flow problems. Implementation on massively parallel architectures, such as GPUs, will also be pursued to decrease computational time.

Bibliography

M Abbaszadeh, M Dehghan, A Khodadadian, and C Heitzinger. Analysis and application of the interpolating element free galerkin (iefg) method to simulate the prevention of groundwater contamination with application in fluid flow. *Journal of Computational and Applied Mathematics*, 368:112453, 2020.

Paola F Antonietti and Giorgio Pennesi. V-cycle multigrid algorithms for discontinuous Galerkin methods on non-nested polytopic meshes. *Journal of Scientific Computing*, 78 (1):625–652, 2019.

I Babuška and JM Melenk. The partition of unity method. *International Journal for numerical methods in engineering*, 40(4):727–758, 1997.

Leonard Bairstow and Arthur Berry. Two-dimensional solutions of Poisson's and Laplace's equations. *Proceedings of the Royal Society of London. Series A, Containing Papers of a Mathematical and Physical Character*, 95(672):457–475, 1919.

Gregory Allen Barnett. *A robust RBF-FD formulation based on polyharmonic splines and polynomials*. PhD thesis, PhD thesis, University of Colorado Boulder, 2015.

Francesco Bassi, Lorenzo Botti, Alessandro Colombo, Daniele A Di Pietro, and Pietro Tesini. On the flexibility of agglomeration based physical space discontinuous galerkin discretizations. *Journal of Computational Physics*, 231(1):45–65, 2012.

Harry Bateman. A partial differential equation associated with Poisson's work on the theory of sound. *American Journal of Mathematics*, 60(2):293–296, 1938.

V Bayona. Comparison of moving least squares and rbf+ poly for interpolation and derivative approximation. *Journal of Scientific Computing*, 81(1):486–512, 2019.

V Bayona, N Flyer, B Fornberg, and GA Barnett. On the role of polynomials in RBF–FD approximations: II. Numerical solution of elliptic PDEs. *Journal of Computational Physics*, 332:257–273, 2017.

T Belytschko, YY Lu, and L Gu. Element-free Galerkin methods. *International Journal for numerical methods in engineering*, 37(2):229–256, 1994.

Marco L Bittencourt, Craig C Douglas, and Raúl A Feijóo. Nonnested multigrid methods for linear problems. *Numerical Methods for Partial Differential Equations: An International Journal*, 17(4):313–331, 2001.

Marco L Bittencourt, Craig C Douglas, and Raúl A Feijóo. Adaptive non-nested multigrid methods. *Engineering Computations*, 19(2):158–176, 2002.

B Boroomand, M Najjar, and Eugenio Oñate. The generalized finite point method. *Computational Mechanics*, 44(2):173–190, 2009.

Achi Brandt. Multi-level adaptive solutions to boundary-value problems. *Mathematics of Computation*, 31(138):333–390, 1977.

Achi Brandt. Algebraic multigrid theory: The symmetric case. *Applied Mathematics and Computation*, 19(1-4):23–56, 1986.

William L Briggs, Van Emden Henson, and Steve F McCormick. *A multigrid tutorial*. SIAM, 2000.

Martin D Buhmann. *Radial basis functions: Theory and implementations*, volume 12. Cambridge University Press, 2003.

Gilles Carré. An implicit multigrid method by agglomeration applied to turbulent flows. *Computers & Fluids*, 26(3):299–320, 1997.

Tony F Chan, Jinchao Xu, and Ludmil Zikatanov. An agglomeration multigrid method for unstructured grids. *Contemporary Mathematics*, 218:67–81, 1998.

Y Chen, J Lee, and A Eskandarian. An overview on meshless methods and their applications. *Meshless Methods in Solid Mechanics*, pages 55–67, 2006.

Elizabeth Cuthill and James McKee. Reducing the bandwidth of sparse symmetric matrices. pages 157–172. ACM: Proceedings of the 24th national conference, 1969.

JE Dendy. Black box multigrid. *Journal of Computational Physics*, 48(3):366–386, 1982.

CA Duarte. *The hp cloud method*. PhD thesis, University of Texas at Austin USA, 1996.

CA Duarte and JT Oden. An hp adaptive method using clouds. *Computer Methods in Applied Mechanics and Engineering*, 139(1-4):237–262, 1996.

Howard C Elman, Oliver G Ernst, and Dianne P O'Leary. A multigrid method enhanced by Krylov subspace iteration for discrete Helmholtz equations. *SIAM Journal on Scientific Computing*, 23(4):1291–1315, 2001.

Yogi A Erlangga, Cornelis W Oosterlee, and Cornelis Vuik. A novel multigrid based preconditioner for heterogeneous Helmholtz problems. *SIAM Journal on Scientific Computing*, 27(4):1471–1492, 2006.

Nikolay M Evstigneev. Numerical analysis of Krylov multigrid methods for stationary advection-diffusion equation. In *Journal of Physics: Conference Series*, volume 1391, page 012080. IOP Publishing, 2019.

N Flyer, B Fornberg, V Bayona, and GA Barnett. On the role of polynomials in RBF–FD approximations: I. Interpolation and accuracy. *Journal of Computational Physics*, 321: 21–38, 2016.

Richard Franke and Greg Nielson. Smooth interpolation of large sets of scattered data. *International Journal for Numerical Methods in Engineering*, 15(11):1691–1704, 1980.

L Gavete, F Ureña, JJ Benito, A García, M Ureña, and E Salete. Solving second order non-linear elliptic partial differential equations using generalized finite difference method. *Journal of Computational and Applied Mathematics*, 318:378–387, 2017.

Christophe Geuzaine and Jean-François Remacle. Gmsh: A 3D finite element mesh generator with built-in pre-and post-processing facilities. *International Journal for Numerical Methods in Engineering*, 79(11):1309–1331, 2009.

G Guennebaud, B Jacob, et al. Eigen v3, 2020. URL `http://eigen.tuxfamily.org`.

D Gunderman, N Flyer, and B Fornberg. Transport schemes in spherical geometries using spline-based rbf-fd with polynomials. *Journal of Computational Physics*, page 109256, 2020.

Rolland L Hardy. Multiquadric equations of topography and other irregular surfaces. *Journal of Geophysical Research*, 76(8):1905–1915, 1971.

Francis H Harlow and J Eddie Welch. Numerical calculation of time-dependent viscous incompressible flow of fluid with free surface. *Physics of Fluids*, 8(12):2182–2189, 1965.

T Huang. *A Stabilized Reproducing Kernel Formulation for Shock Modeling in Fluids and Fluid-Structure Interactive Systems*. PhD thesis, UC San Diego, 2020.

BR Hutchinson, PF Galpin, and GD Raithby. Application of additive correction multigrid to the coupled fluid flow equations. *Numerical Heat Transfer*, 13(2):133–147, 1988.

M Jančič, J Slak, and G Kosec. Analysis of high order dimension independent rbf-fd solution of poisson's equation. *arXiv preprint arXiv:1909.01126*, 2019.

Volker John and Lutz Tobiska. Numerical performance of smoothers in coupled multigrid methods for the parallel solution of the incompressible Navier–Stokes equations. *International Journal for Numerical Methods in Fluids*, 33(4):453–473, 2000.

Edward J Kansa. Multiquadrics—a scattered data approximation scheme with applications to computational fluid-dynamics—i surface approximations and partial derivative estimates. *Computers & Mathematics with Applications*, 19(8-9):127–145, 1990a.

Edward J Kansa. Multiquadrics—a scattered data approximation scheme with applications to computational fluid-dynamics—ii solutions to parabolic, hyperbolic and elliptic partial differential equations. *Computers & Mathematics with Applications*, 19(8-9):147–161, 1990b.

EJ Kansa. Multiquadrics—A scattered data approximation scheme with applications to computational fluid-dynamics—I surface approximations and partial derivative estimates. *Computers & Mathematics with Applications*, 19(8-9):127–145, 1990c.

EJ Kansa. Multiquadrics—A scattered data approximation scheme with applications to computational fluid-dynamics—II solutions to parabolic, hyperbolic and elliptic partial differential equations. *Computers & Mathematics with Applications*, 19(8-9):147–161, 1990d.

EJ Kansa and YC Hon. Circumventing the ill-conditioning problem with multiquadric radial basis functions: applications to elliptic partial differential equations. *Computers & Mathematics with Applications*, 39(7-8):123–137, 2000.

Aaron Katz and Antony Jameson. Multicloud: Multigrid convergence with a meshless operator. *Journal of Computational Physics*, 228(14):5237–5250, 2009.

Bruno Koobus, Marie-Hélène Lallemand, and Alain Dervieux. Unstructured volume-agglomeration mg: Solution of the Poisson equation. *International Journal for Numerical Methods in Fluids*, 18(1):27–42, 1994.

LIG Kovasznay. Laminar flow behind a two-dimensional grid. In *Mathematical Proceedings of the Cambridge Philosophical Society*, volume 44, pages 58–62. Cambridge University Press, 1948.

Marie-Helene Lallemand, Herve Steve, and Alain Dervieux. Unstructured multigridding by volume agglomeration: Current status. *Computers & Fluids*, 21(3):397–433, 1992.

Stefan Langer. Agglomeration multigrid methods with implicit runge–kutta smoothers applied to aerodynamic simulations on unstructured grids. *Journal of Computational Physics*, 277:72–100, 2014.

T Liszka and J Orkisz. The finite difference method at arbitrary irregular grids and its application in applied mechanics. *Computers & Structures*, 11(1-2):83–95, 1980.

TJ Liszka, CAM Duarte, and WW Tworzydlo. hp-meshless cloud method. *Computer Methods in Applied Mechanics and Engineering*, 139(1):263–288, 1996.

WK Liu, S Jun, and YF Zhang. Reproducing kernel particle methods. *International Journal for numerical methods in fluids*, 20(8-9):1081–1106, 1995.

Dimitri J Mavriplis and Antony Jameson. Multigrid solution of the Navier-Stokes equations on triangular meshes. *AIAA Journal*, 28(8):1415–1425, 1990.

DJ Mavriplis and V Venkatakrishnan. A 3D agglomeration multigrid solver for the Reynolds–averaged Navier–Stokes equations on unstructured meshes. *International Journal for Numerical Methods in Fluids*, 23(6):527–544, 1996.

JM Melenk and I Babuška. The partition of unity finite element method: basic theory and applications. In *Research Report/Seminar für Angewandte Mathematik*, volume 1996. Eidgenössische Technische Hochschule, Seminar für Angewandte Mathematik, 1996.

JJ Monaghan. Smoothed particle hydrodynamics and its diverse applications. *Annual Review of Fluid Mechanics*, 44:323–346, 2012.

E Oñate, S Idelsohn, OC Zienkiewicz, and RL Taylor. A finite point method in computational mechanics. applications to convective transport and fluid flow. *International Journal for numerical methods in engineering*, 39(22):3839–3866, 1996.

E Oñate, C Sacco, and S Idelsohn. A finite point method for incompressible flow problems. *Computing and visualization in science*, 3(1-2):67–75, 2000.

MF Paisley. Multigrid solution of the incompressible Navier–Stokes equations for three-dimensional recirculating flow: Coupled and decoupled smoothers compared. *International Journal for Numerical Methods in Fluids*, 30(4):441–459, 1999.

N Perrone and R Kao. A general finite difference method for arbitrary meshes. *Computers & Structures*, 5(1):45–57, 1975.

G Pöplau and U Van Rienen. Multigrid solvers for Poisson's equation in computational electromagnetics. In *Scientific Computing in Electrical Engineering*, pages 169–176. Springer, 2001.

John W Ruge and Klaus Stüben. Algebraic multigrid. In *Multigrid Methods*, pages 73–130. SIAM, 1987.

Youcef Saad and Martin H Schultz. GMRES: A generalized minimal residual algorithm for solving nonsymmetric linear systems. *SIAM Journal on Scientific Computing*, 7(3): 856–869, 1986.

A Settari and K Aziz. A generalization of the additive correction methods for the iterative solution of matrix equations. *SIAM Journal on Numerical Analysis*, 10(3):506–521, 1973.

Shantanu Shahane, Anand Radhakrishnan, and Surya Pratap Vanka. A high-order accurate meshless method for solution of incompressible fluid flow problems. *arXiv preprint arXiv:2010.01702*, 2020.

Varun Shankar. The overlapped radial basis function-finite difference (RBF-FD) method: A generalization of RBF-FD. *Journal of Computational Physics*, 342:211–228, 2017.

Masayoshi Shimada, Hiroshi Tokunaga, Nobuyuki Satofuka, and Hidetoshi Nishida. Numerical simulation of three-dimensional viscous flows using the vector potential method. *JSME international journal. Ser. 2, Fluids engineering, heat transfer, power, combustion, thermophysical properties*, 34(2):109–114, 1991.

C Shu, H Ding, and KS Yeo. Local radial basis function-based differential quadrature method and its application to solve two-dimensional incompressible Navier–Stokes equations. *Computer Methods in Applied Mechanics and Engineering*, 192(7-8):941–954, 2003.

S Sivaloganathan and GJ Shaw. A multigrid method for recirculating flows. *International Journal for Numerical Methods in Fluids*, 8(4):417–440, 1988.

Klaus Stüben and Ulrich Trottenberg. Multigrid methods: Fundamental algorithms, model problem analysis and applications. *Multigrid Methods*, pages 1–176, 1982.

MC Thompson and Joel H Ferziger. An adaptive multigrid technique for the incompressible Navier-Stokes equations. *Journal of Computational Physics*, 82(1):94–121, 1989.

A Tiwari and SP Vanka. A ghost fluid lattice boltzmann method for complex geometries. *International Journal for Numerical Methods in Fluids*, 69(2):481–498, 2012.

Ulrich Trottenberg, Cornelius W Oosterlee, and Anton Schuller. *Multigrid*. Elsevier, 2000.

S Pratap Vanka. Block-implicit multigrid solution of Navier-Stokes equations in primitive variables. *Journal of Computational Physics*, 65(1):138–158, 1986.

V Venkatakrishnan and Dimitri J Mavriplis. Agglomeration multigrid for the three-dimensional Euler equations. *AIAA journal*, 33(4):633–640, 1995.

Roman Wienands, Cornelis W Oosterlee, and Takumi Washio. Fourier analysis of GMRES (m) preconditioned by multigrid. *SIAM Journal on Scientific Computing*, 22(2):582–603, 2000.

Jinchao Xu. The auxiliary space method and optimal multigrid preconditioning techniques for unstructured grids. *Computing*, 56(3):215–235, 1996.

Ulrike Meier Yang et al. BoomerAMG: A parallel algebraic multigrid solver and preconditioner. *Applied Numerical Mathematics*, 41(1):155–177, 2002.

Irad Yavneh. Why multigrid methods are so efficient. *Computing in Science & Engineering*, 8(6):12–22, 2006.

T Ye, D Pan, C Huang, and M Liu. Smoothed particle hydrodynamics (sph) for complex fluid flows: Recent developments in methodology and applications. *Physics of Fluids*, 31 (1):011301, 2019.

A Zhang, P Sun, F Ming, and A Colagrossi. Smoothed particle hydrodynamics and its applications in fluid-structure interactions. *Journal of Hydrodynamics*, 29(2):187–216, 2017.

L Zhang, J Ouyang, and X Zhang. On a two-level element-free galerkin method for incompressible fluid flow. *Applied Numerical Mathematics*, 59(8):1894–1904, 2009.